Journal for ImmunoTherapy of Cancer

Conformation-sensitive targeting of CD18 depletes M2-like tumor-associated macrophages resulting in inhibition of solid tumor progression

Ik-Hwan Han,[1] Ilseob Choi ,[1,2] Hongseo Choi,[3] Soyoung Kim,[1,2] Chanmi Jeong,[1,2] Juwon Yang,[1] Yingying Cao,[4] Jeongyoon Choi,[3] Heekyung Lee,[3] Jin Sun Shin,[3] Hye Duck Yeom,[5] Eun-Ji Lee,[6] Nari Cha,[1,2] Hyemin Go,[7] Se Eun Lim,[7] Songah Chae,[7] Won-Jun Lee,[7] Minjin Kwon,[7] Hongsung Kim,[7] Hyojung Choi,[7] Sehyun Pak,[7] Namgyeong Park,[8] Eunbin Ko,[8] Deok-Sang Hwang,[8] Junho H Lee,[9] Hwan-Suck Chung,[6] Seong Ho Kang,[10] Hyunsu Bae [1,2]

To cite: Han I-H, Choi I, Choi H, *et al*. Conformation-sensitive targeting of CD18 depletes M2-like tumor-associated macrophages resulting in inhibition of solid tumor progression. *Journal for ImmunoTherapy of Cancer* 2025;**13**:e011422. doi:10.1136/jitc-2024-011422

► Additional supplemental material is published online only. To view, please visit the journal online (https://doi.org/10.1136/jitc-2024-011422).

I-HH and IC contributed equally.

I-HH and IC are joint first authors.

Accepted 23 March 2025

For numbered affiliations see end of article.

Correspondence to
Dr Hyunsu Bae; hbae@khu.ac.kr

Professor Seong Ho Kang; shkang@khu.ac.kr

ABSTRACT

Background Tumor-associated macrophages (TAMs) primarily exist in the M2-like phenotype in the tumor microenvironment (TME). M2-TAMs contribute to tumor progression by establishing an immunosuppressive environment. However, TAM targeting is hindered, mainly owing to a lack of specific biomarkers for M2-TAMs. Previously, we demonstrated that a novel peptide drug conjugate (TB511) consisting of a TAM-binding peptide and the apoptosis-promoting peptide targets M2-TAMs. This was achieved through M2-TAM targeting, although the target mechanism of action remained elusive. Herein, we elucidate the anticancer efficacy of TB511 by identifying new target proteins that preferentially bind to M2-TAMs and clarifying the apoptosis-inducing mechanism in these cells.

Methods We investigated the target proteins and binding site of TB511 using LC-MS/MS analyses, surface plasmon resonance and peptide–protein interaction 3D modeling. Activated CD18 expression in M2 TAMs was assessed using Quantibrite PE beads in PBMCs. The anticancer efficacy of TB511 was tested using colorectal cancer (CRC) and non-small cell lung cancer (NSCLC) mouse model. The immunotherapeutic effect of TB511 was investigated through spatial transcriptomics in human pancreatic ductal adenocarcinoma (PDAC) model.

Results Activated CD18 was highly expressed in human tumor tissues and was significantly higher in M2 TAMs than in other immune cells. TB511 showed high binding affinity to CD18 among the cell membrane proteins of M2 macrophages and appeared to bind to the cysteine-rich domain in the activated form. Moreover, TB511 specifically induced apoptosis in M2 TAMs, but its targeting ability to M2 macrophages was inhibited in CD18 blockade or knockout model. In mouse or humanized mouse models of solid tumors such as CRC, NSCLC, and PDAC, TB511 suppressed tumor growth by targeting M2-TAMs via CD18 and enhancing the presence of $CD8^+$ T cells in the TME.

Conclusions Collectively, our findings suggest that activated CD18 holds promise as a novel target protein for cancer therapy, and TB511 shows potential as a therapeutic agent for tumor treatment.

WHAT IS ALREADY KNOWN ON THIS TOPIC

⇒ Tumor-associated macrophages (TAMs), particularly M2-like TAMs, contribute to tumor progression by creating an immunosuppressive microenvironment. However, targeting M2-TAMs remains challenging due to the lack of specific biomarkers.

WHAT THIS STUDY ADDS

⇒ This study identifies activated CD18 as a novel target protein highly expressed in M2-TAMs and demonstrates that TB511, a peptide drug conjugate, specifically binds to the cysteine-rich domain of activated CD18. TB511 effectively induces apoptosis in M2-TAMs and enhances $CD8^+$ T cell infiltration in the tumor microenvironment, leading to suppressed tumor growth in colorectal cancer, non-small cell lung cancer, and pancreatic ductal adenocarinoma models.

HOW THIS STUDY MIGHT AFFECT RESEARCH, PRACTICE OR POLICY

⇒ By establishing activated CD18 as a specific marker for M2-TAMs, this study provides a new direction for macrophage-targeted cancer immunotherapy. TB511's mechanism of action supports the development of selective TAM-targeting therapies, which could be integrated into existing immunotherapy regimens. These findings may influence future research on tumor immunology and inform therapeutic strategies for solid tumors resistant to conventional treatments.

INTRODUCTION

The tumor microenvironment (TME) plays a pivotal role in the behavior and development of solid tumors.[1] Notably, tumor-associated

macrophages (TAMs) suppress the recruitment and activity of tumor-killing cells such as $CD8^+$ T and natural killer (NK) cells in the TME.[2–4] Consequently, reprogramming of the TME by targeting immunosuppressive cells has emerged as an attractive research paradigm and has garnered significant clinical interest.[5]

TAMs are major tumor-infiltrating immune cells that constitute up to 50% of the tumor mass.[6] These highly plastic cells primarily exist as M1-TAMs and M2-TAMs. While M1-TAMs kill tumor cells or secrete immunostimulatory cytokines to enhance the cytotoxic function of other leucocytes, M2-TAMs interact with tumor cells to enhance the immunosuppressive environment within the TME and contribute to all aspects of tumor progression. A high density of M2-TAMs within the TME is associated with poor prognosis in solid tumors.[7] Therefore, targeting M2-TAMs may be an attractive anticancer strategy. However, the lack of specific markers for M2-TAMs has hampered the development of selective drugs that target M2-TAMs.

CD18 (ITGB2) is a complex leucocyte-specific adhesion molecule that plays a crucial role in cell adhesion and migration. CD18 combines with α subunits (CD11a, CD11b, CD11c, and CD11d) and forms heterodimers such as lymphocyte factor 1 (LFA-1, CD11a/CD18), macrophage-1 antigen (Mac-1, CD11b/CD18), complement receptor 4 (CR4, CD11c/CD18), and CD11d/CD18.[8] CD18 undergoes a conformational change from a bent closed conformation to an extended open conformation on activation, which is critical for leucocyte adhesion. Circulating leucocytes in the blood predominantly express CD18 in an inactive state. However, during the inflammatory response and in the presence of chemokines, CD18 is activated, leading to leucocyte adhesion.[9 10] The TME contains abundant chemokines and extracellular matrix proteins that induce Mac-1 activation.[11 12] High expression of CD18 has been shown to correlate negatively with patient survival and is associated with poor prognosis in various solid tumors.[13–15] Therefore, CD18, with its open conformation, can be an ideal drug target for M2-TAMs in the TME and a promising strategy for treating solid tumors.

Peptide-drug conjugate (PDC) is a promising treatment method for targeted delivery of drugs to specific cells or tissues by chemically linking a peptide that selectively binds to target cells and a drug that induces cell death.[16 17] In the context of cancer immunotherapy, PDCs are developing as powerful tools to selectively modulate the TME.[18] Recently, PDCs are being developed that can specifically target M2-like TAMs, which play a key role in tumor progression and immune evasion. However, despite these promising advances, the field of PDC is still in its infancy, and there are many challenges to overcome.[19 20] One such challenge is efficient transport of PDCs across biological barriers, which is critical for therapeutic efficacy.[21] This requires further research into peptide carriers that could potentially be used to enhance PDC delivery.[22] In previous studies, we developed a peptide (TAMpep) that preferentially binds to M2 macrophages.[23] However, their binding mechanism was unclear.

This study aimed to identify the target and precise mechanism of action of PDC (TB511), comprising a TAM-binding peptide (TAMpep) and a pro-apoptotic peptide (dKLA), in solid tumor models including lung and colon cancer. The findings of this study could provide valuable insights for future clinical therapies. Specifically, comprehending the conformational changes of CD18 in M2 TAMs within the TME is crucial for elucidating its correlation with tumor progression and recognizing its potential as a significant target protein for cancer therapy; the findings of this study could provide valuable insights for future clinical therapies.

MATERIALS AND METHODS

Peptide synthesis

Peptides used in this study were synthesized by GenScript (Piscataway, New Jersey, USA) and are detailed in online supplemental table S1. All peptides were purified to greater than 95% purity. Moreover, the structure of TB511 was analyzed using Fourier-transform infrared spectroscopy and Circular Dichroism (CD) spectroscopy.

Immunofluorescence staining

The tumor tissues were fixed overnight in 10% neutral-buffered formalin. After embedding in paraffin, tumor tissues were cut into 5 µm of regular thickness. The slides were deparaffinized in xylene and dehydrated in ethanol and deionized water. For antigen retrieval, slides were incubated in sodium citrate buffer (pH 6.0) for 15 min in a microwave. The slides were then incubated with a peroxidase-blocking solution (Dako, Glostrup, Denmark) for 15 min and blocked with 5% bovine serum albumin. Slides were incubated with primary antibodies overnight, washed with Tris-buffered saline (TBS) containing 0.1% Tween20. Slides were then incubated with primary antibodies overnight at 4°C. Slides were then stained with FITC-labeled TAMpep and APC-conjugated anti-rabbit IgG secondary antibody (Invitrogen) at 37°C for 1 hour. To visualize the nuclei, the cover glasses were mounted with Vectashield mounting medium (Vector Laboratories) with 4′,6-diamidino-2-phenylindole. Images were captured using the LSM 800 confocal laser-scanning microscope (Carl Zeiss, Oberkochen, Germany). The antibodies used are listed in online supplemental table S2.

Annexin V assay

THP-1 cells or Jurkat were incubated with 1 mM Mn^{2+} for 1 hour at 37°C for CD18 activation. The activated cells were incubated with 1 µM TB511 for 1 hour at 37°C and then cultured in serum-free medium for 24 hours. Cells were harvested and stained with APC-conjugated Annexin V (Invitrogen) for 15 min at RT. After centrifugation at 300×g for 5 min at 4°C, cells were treated with

7-AAD Viability Staining Solution (Invitrogen) containing BD Pharmingen Stain Buffer (FBS) (BD Bioscience). All data were acquired using FACSLyric (BD Bioscience) and analyzed using FACSuite software (BD Bioscience).

Live cell imaging fluorescence microscopy

To measure apoptosis induced by TB511, THP-1 cells were seeded at 2×10^4 cells/well in 96-well plates and differentiated into M0, M1, M2, or TAMs. Differentiated cells were treated with MitoTracker RedROX (Invitrogen) and a caspase 3/7 reagent for 30 min. Next, the cells were treated with TB511 (1 µM) and then immediately evaluated using restoration fluorescence microscopy (DeltaVison, New Jersey, USA).

Biotin pull-down assay

Lysates of M2-differentiated THP-1 cells were obtained using a Membrane Protein Extraction Kit (Thermo Fisher Scientific). Cell lysates were incubated with scrambled and TAMpep peptides (0, 0.001, 0.01, 0.1, 1, and 10 µg) and then with biotinylated TAMpep for 1 hour at 4°C with shaking. After incubation, the peptide-bound membrane proteins were eluted using streptavidin Dynabeads (Thermo Fisher Scientific). Eluted proteins were loaded onto a 10% sodium dodecyl sulfate-polyacrylamide gel and transferred onto polyvinylidene difluoride membranes. The membrane was blocked and incubated with anti-CD18 antibody (LSbio) overnight at 4°C. After washing with TBS containing 25 mM Tris-Cl, 150 mM NaCl, and 0.05% Tween-20, the membranes were incubated with anti-rabbit horseradish peroxidase-conjugated secondary antibodies. Protein bands were visualized using a Western Blotting Detection Reagent Kit (Thermo Fisher Scientific) and analyzed using ImageJ software (NIH, Bethesda, Maryland, USA).

Surface plasmon resonance

The binding affinity of total CD18 (Prospec), the I-domain (Cloud-Clone), the cys-rich domain (Cloud-Clone), and recombinant Myelin Basic Protein (MBP; Cloud-Clone, #RPA539Mu01) to TAMpep was measured using surface plasmon resonance (SPR) on a Biacore T200 system (GE Healthcare, Freiburg, Germany). Before the experiment, the surface of the series S sensor chip SA was cleaned with injections of 1 M NaCl and 50 mM NaOH solutions, three times for 1 min each. TAMpep (10 nM) was immobilized on the SA chip surface at a flow rate of 10 µL/min. The surface was subsequently washed with 50% isopropanol, 1 M NaCl, and 50 mM NaOH to remove non-specific binding. For the analyte binding studies, total CD18, I-domain, cys-rich domain, and MBP protein were prepared at concentrations achieving saturated responses below 150 response units (RU). Each analyte was then serially diluted (twofold) four to five times. The multicycle analysis method was used to inject different concentrations of analytes at a flow rate of 30 µL/min to measure binding kinetics. Kinetic data were analyzed using BIA evaluation software (V.3.2.1, GE Healthcare), and the equilibrium dissociation constant (KD) was calculated as KD=kd/ka, where ka is the association rate constant and kd is the dissociation rate constant. Confidence in the results was validated by U-values (<15) for all analyses, except for total CD18.

Immunohistochemistry

For histological analysis, the brain, breast, colon, kidney, liver, lung, skin, and tumor tissues were fixed overnight in 10% neutral-buffered formalin. After embedding in paraffin, tumor tissues were cut into 4 µm of regular thickness. The slides were deparaffinized in xylene and dehydrated in ethanol and deionized water. For antigen retrieval, slides were incubated in sodium citrate buffer (pH 6.0) for 15 min in a microwave. The slides were then incubated with a peroxidase-blocking solution (Dako, Glostrup, Denmark, #S202386) for 15 min and blocked with 5% bovine serum albumin. Slides were incubated with primary antibodies overnight, washed with TBS containing 0.1% Tween20, incubated with an avidin-biotin complex kit (Vector Laboratories, Burlingame, CA, USA; #PK-6101), and visualized by incubation with diaminobenzidine-HCL (Vector laboratories, #SK4100). Nuclei were counterstained with hematoxylin. Slides were observed under a bright-field microscope (Nikon, Tokyo, Japan) and analyzed using ImageJ software (NIH). Antibodies used for immunohistochemistry (IHC) staining are listed in the online supplemental table S2.

Modeling of protein-peptide interactions

Based on the sequence of the cysteine-rich region of CD18 (Uniport _p05107, cysteine-rich tandem repeat region: 449-617), a tertiary structure was constructed using the trRosetta algorithm (https://yanglab.nankai.edu.cn/trRosetta/). Docking simulations of TB511 and CD18 were performed using the CABS-dock server (http://biocomp.chem.uw.edu.pl/CABSdock/) with the CD18 PDB file generated using trRosetta and the amino acid sequence of TB511. Among the 10 models created from the docking simulation, a representative model was selected based on the results of alanine substitutions in the TB511 sequence.

Single particle tracking imaging

TB511-AuNRs were synthesized with AuNRs and indicated in online supplemental methods. THP-1 cells were seeded on 22×22 mm coverslips (No. 1, Deckglaser, Freiburg, Germany) and housed in Petri dishes. After differentiating into M2 macrophages, the concentration of TB511-AuNRs was adjusted to ~1.5×10^9 particles/mL. The cells were incubated with 20 µL of TB511-AuNRs for 1 hour, followed by incubation with MitoTracker Green (Invitrogen) and Hoechst 33342 (Invitrogen) for 0.5 hour. An 18×18 mm coverslip was attached to the cell coverslip using double-sided tape. The space was filled with a cell culture medium to sustain the cells. Then, single particle tracking images were acquired with a 10 ms interval by integrated multidimensional light-sheet

microscopy (*i*MLSM). An Olympus BX53 upright microscope was used to construct the *i*MLSM.[24] ImageJ (NIH) and MATLAB (Mathworks, Torrance, California, USA) were used to analyze the acquired images. The 3D spatial trajectories (x, y, z) of individual peptide-AuNRs were super-localized with the astigmatism method.[25 26] The rotations and orientations of individual peptide-AuNRs were calculated by fitting $\cos^2\varphi$ for transverse SPR and $\sin^2\theta$ for longitudinal SPR.[27]

Animal study

To create a subcutaneous lung cancer mouse model, tumor cells were resuspended in a serum-free medium and mixed with 1:1 Matrigel (Corning, New York, USA). LLC cells were subcutaneously inoculated into the right flank of 6–8 weeks old C57BL/6 (Taconic Biosciences, New York, USA). When the tumor volume reached 50–100 mm^3, the tumor-bearing mice were divided into two groups. TB511 has shown plasma stability for approximately 60 hours; therefore, it was administered every 3 days in the tumor mouse model. TB511 was injected subcutaneously at a dose of 200 nmol/kg every 3 days. Tumor diameters were measured using a digital caliper, and tumor volume was calculated according to the following formula: (length×width^2)/2. All animal studies were terminated when the tumor volume reached <2000 mm^3. For the orthotopic mouse model, the fur in the abdominal area of the mice was shaved with clippers, and the mice were anesthetized with isoflurane. The abdomen of the mice was excised using a sterile surgical scalpel, and CT-26 Luc cells were injected into the subserosal plane of the cecum. The surgical incision site was closed using sutures. 7 days after tumor inoculation, the mice were randomly divided into two groups. TB511 was injected subcutaneously every 3 days. D-luciferin (BioVision, Milpitas, California, USA) was injected intraperitoneally at a dose of 3 mg/mouse to track tumor growth. Mice were evaluated using the NightOWL LB 983 in vivo imaging system (Berthold Technologies, Bad Wildbad, Germany) once a week. All mice were sacrificed, and tumor tissues were isolated.

To assess whether CD18 is a target protein of TB511, BALB/c wild-type (WT) mice and CD18 knockout mice (C.129S7(B6)-Itgb2^{tm2Bay}/AbhmJ, 6–8 weeks old) were purchased from the Jackson Laboratory. For the subcutaneous mouse model of lung cancer, LLC cells were inoculated with 1×10^6 cells per mouse into the right flank. After 7 days, TB511 was subcutaneously administered twice per week. The tumor volume was measured twice weekly using a digital caliper. The mice were euthanized after four injections. In an orthotopic mouse model of colorectal cancer (CRC), CT26-luc cells were injected into the subserosal plane of the cecum. After 7 days, TB511 was subcutaneously injected every 3 days and the tumor volume was measured weekly using an in vivo imaging system. The mice were sacrificed after 4 weeks, and the tumor tissues were extracted.

Generation of humanized tumor mice model

SID mice (NOD-Prkdc^{em1Beak}IL2rg^{em1Break}, 4-week-old) were purchased from the GemBioscience (Chungbuk, Korea).[28] Mice were irradiated with 1.5 Gy of γ-rays and were intravenously injected with human CD34$^+$ hematopoietic stem cells (2×10^5 cells/mouse, Lonza, Basel, Switzerland). After 11 weeks, mouse peripheral blood was obtained, and the engraftment of mature human white blood cells (human CD45$^+$ cells) was confirmed using flow cytometry. Humanized mice were considered to have more than 25% human CD45 cells in their peripheral blood; the hCD45$^+$ cell population accounted for 37.32%±13.44% in 16 male mice and 42.63%±10.41% in 15 female mice 11 weeks after engraftment. A549, a human lung cancer cell line, and PANC1, a human pancreatic cancer cell line, were subcutaneously injected into the right flank of humanized mice. When the tumor volume reached 50–100 mm^3, PBS or TB511 was subcutaneously injected, and the tumor volume was measured every 3 days. At the end of the animal study, the mice were sacrificed, and tumor tissues were extracted to analyze the changes in immune cells in the TME.

Flow cytometry analysis

Tumor tissues were minced into thin pieces using a MACS dissociator (Milteny Biotec, Auburn, California, USA) and incubated with 1 U/mL DNase I (Roche, Indianapolis, Indiana, USA) and 1 mg/mL collagenase D (Roche) in RPMI 1640 serum-free media for 30 min at 37°C. The tissue was filtered through a 100 µm nylon mesh strainer. The RBCs in the filtered single cells were lysed with BD Pharm lyse buffer (BD Bioscience, California, USA). The single cells were then stained with BD Pharmingen Stain Buffer (BD Bioscience) with antibodies, which are listed in online supplemental table S3. The cells were detected using a FACS Lyric System (BD Bioscience) and analyzed using FlowJo software (BD Bioscience).

To evaluate CD18-activated macrophages in tissues, the brain, breast, colon, kidney, liver, lung, skin, and tumor tissues were made into single cells. The single cells were then stained with antibodies, which are listed in online supplemental table S3. The cells were detected using a FACS Lyric System (BD Bioscience) and analyzed using FlowJo software (BD Bioscience).

For assessing CD18 and KIM127 target levels, flow cytometric analysis was performed using a BD FACSLyric flow cytometer (BD Bioscience; equipped with six lasers—510, 525, 575, 774, 603, and 421 nm) with FlowJo software (BD Bioscience). To estimate the absolute number of membrane-bound CD18 and KIM127 molecules, we used Quantibrite beads (information provided with Quantibrite PE beads). The analysis of Quantibrite PE calibration beads is Log10 values for PE fluorescence geometric means and for values of PE molecules per were calculated. Using the values obtained, we plotted the log10 values for the number of PE molecules per bead against the log10 values for fluorescence intensity. Given that the PE/antibody ratio was 1:1, PE/antibody values could

be converted to antibody/cell values, which represented the number of receptors per cell. We gated the populations to be analyzed on the basis of indices of forward and side scattering (FSC-A/SSC-A dot plot) that were located within the leucocytic regions. Subsequently, we gated subpopulations of $CD4^+$T lymphocytes or $CD8^+$ T lymphocytes and $CD11b^+$macrophage (dot plots APC-A/FITC-A and APC-A/PE-Cy7-A) on the basis of markers of the different subpopulations. A minimum of 10 000 events were gated.

Spatial transcriptomics

Paraffin-embedded blocks were carefully sectioned at a thickness of 5 µm and mounted onto a Xenium slide. The sectioned slide was incubated for 3 hours at 42°C on a thermal cycler (C1000 96-well, Bio-Rad) for drying. Deparaffinization and de-crosslinking were performed. After prime hybridization and RNase treatment, the sectioned slide was hybridized with the Xenium human 5 k pan-tissue probes (10 x Genomics) at 50°C overnight (~24 hours). The sectioned slide was then washed, and ligation was performed at 42°C for 30 min. Amplification enhancement and amplification were immediately processed on the thermal cycler (C1000 96-well, Bio-Rad). The sectioned slide was then washed, and cell segmentation staining probes were applied to the slide at 4°C overnight (~24 hours). Following stain enhancement and washing, autofluorescence quenching and nuclei staining were performed on the sectioned slide. Subsequently, the sectioned slide was loaded onto the Xenium analyzer (XOA V.3.0.2, 10x Genomics) to begin fluorescence signal detection. After the Xenium run, raw data was preprocessed with xeniumranger V.3.0.0.

Statistics

All data are presented as the mean and SEMs. Statistical significance was analyzed using unpaired t-test and one-way analysis of variance (ANOVA) followed by Tukey's post hoc test, and two-way ANOVA followed by Bonferroni post hoc comparisons using Prism software (GraphPad Software, California, USA). A $p<0.05$ was considered statistically significant.

RESULTS

Expression of activated CD18 in M2 TAMs

Numerous studies have highlighted a significant association between CD18 and the progression of solid tumors, particularly in relation to the infiltration of M2 macrophages into tumor tissues.[13–15] We investigated the expression levels of CD18 in macrophage subtypes. Both gene and protein expression of CD18 were significantly higher in M2 macrophages and TAMs compared with M0 and M1 macrophages (figure 1A–C). To determine the correlation between CD18 expression and tumor progression, we conducted an analysis using the Tumor IMmune Estimation Resource analysis and a tumor tissue array. In a human tissue array, the level of CD18 was significantly higher in tumor tissues than in normal tissues, including the breast, colon, lung, liver, kidney, and skin (figure 1D). Analysis of gene expression patterns in various solid tumor tissues revealed that the expression of ITGB2/CD18 genes and marker genes of M2 macrophages (CD163, AGR and TGFb) were upregulated, and there was a significant correlation between the expression of ITGB2/CD18 and MRC1, one of the markers of M2 macrophages (online supplemental figure 1A,B). CD18, known to effectively mediate leucocyte trafficking and immune response, transitions from an inactive to an active form through a conformational change, thereby exhibiting a high affinity for ligands[29] (figure 1E). To determine the difference in the number of activated CD18 molecules per cell in human immune cells, CD4, CD8 T cells, neutrophils, and macrophages derived from human PBMCs were quantified by conjugating PE to the KIM127 antibody, which is known to specifically bind to the activated CD18. As a result, TAMs and M2 macrophages showed higher CD18 expression compared with other immune cells (figure 1F). Activated CD18 showed the highest level in TAMs compared with other cells as well as M2 macrophages (figure 1G). Additionally, the THP-1 derived TAMs exhibited an increased activation level of CD18 among the macrophage lineage cells (online supplemental figure 1C,D). Furthermore, the activation level of CD18 (pan CD18 and KIM127-double positive) in human tissues was significantly elevated in tumor tissues compared with normal tissues in the breast, colon, lung, and liver (figure 1H). Therefore, these results suggest that activated CD18 is highly expressed in M2-TAMs derived from the TME.

CD18 as a target protein of TB511 in M2-TAMs

We developed a PDC (TB511) comprizing TAMpep, a peptide with preferential binding affinity for M2 macrophages, and dKLA, a pro-apoptotic peptide, linked via a GGGGS linker (online supplemental figure 2).[23] However, the precise mechanism by which TB511 selectively targets M2 macrophages remains undisclosed. To elucidate the mechanism of action of TB511, we verified the target proteins of TB511 using immunoprecipitation and a proteomics-based analysis. As a result, 21 cell membrane proteins were identified in M0, M1, and M2 macrophages using LC-MS/MS. Among these proteins, the ITGB2/CD18 protein exhibited preferential binding to biotin-labeled TAMpep (carrier peptide of TB511) in M2 macrophages compared with M0 and M1 macrophages (online supplemental figure 3). The binding of the CD18 protein with TAMpep in cell membrane proteins of M2 macrophages was blocked by preincubation with non-biotinylated TAMpep in a concentration-dependent manner, whereas preincubation with scrambled peptides was not affecting immunoprecipitation (figure 2A). Colocalization of TAMpep and CD18 on M2 macrophages was confirmed by confocal microscopy (figure 2B). To identify the binding domain of CD18, we measured the affinity of TAMpep with the extracellular

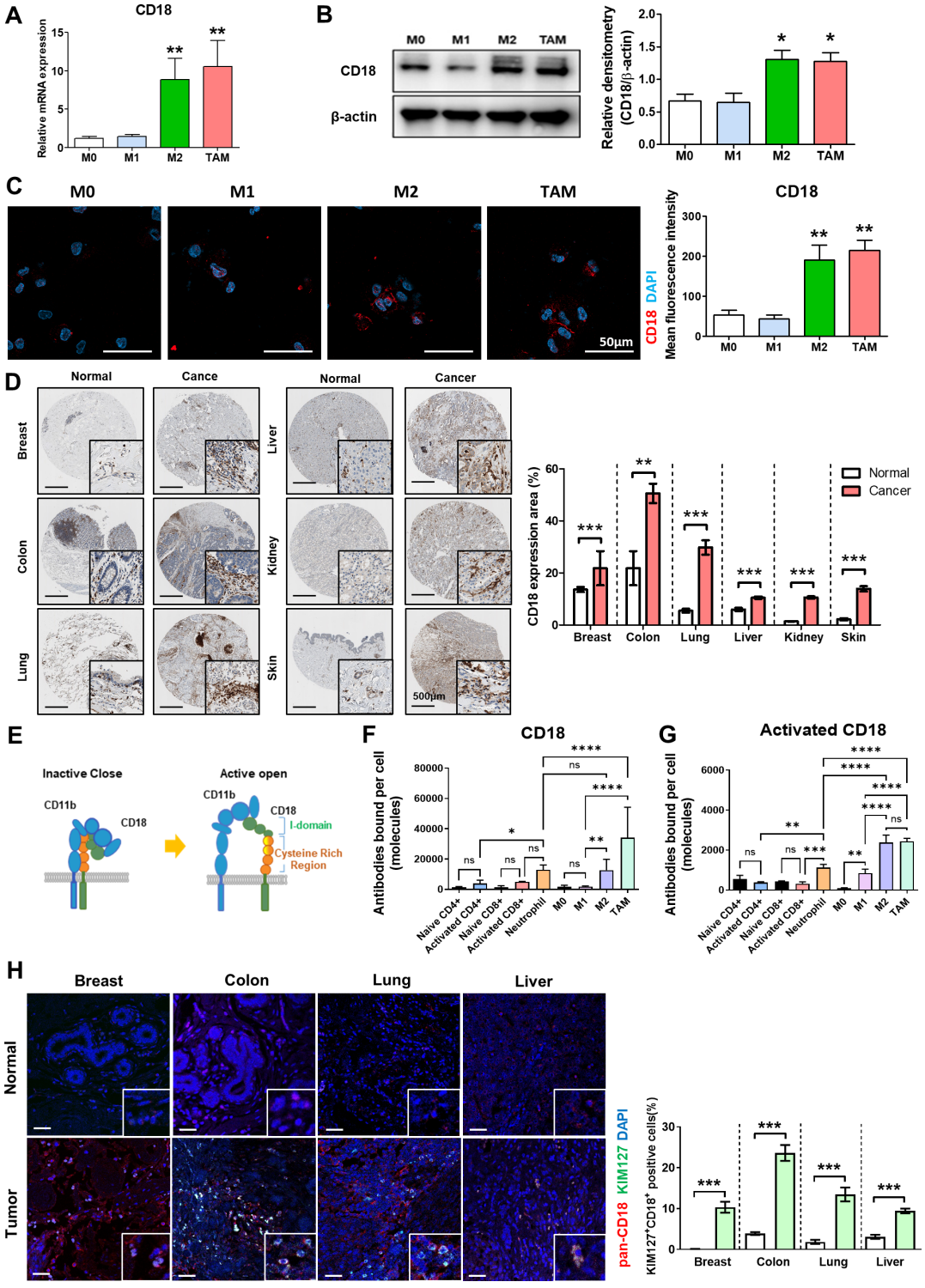

Figure 1 Association of activated CD18 and M2 TAMs in progressed human tumor tissues. (A) The relative mRNA expression levels of CD18 in M0, M1, M2, and M2-TAM macrophages were measured using qRT-PCR. (B) The protein expression levels of CD18 in M0, M1, M2, and M2-TAM were determined using western blotting. (C) Immunostaining images of $CD18^{+}$ cells in M0, M1, M2, and M2-TAM macrophages were marked with CD18 (red) and nuclei (DAPI, blue). (D) Expression of CD18 in various normal and cancerous tissues, including the breast, lung, liver, kidney, and colon was measured using tumor tissue microarrays. CD18 expression was quantified per area (μm^2); scale bar, 500 μm. (E) Schematic diagram illustrating the inactive and active forms of the CD18 protein. (F, G) The degree of expression or activated CD18 on CD4, CD8 T cells, neutrophils, M1, and M2 macrophages derived human PBMCs was measured by staining with anti-CD18 antibody and KIM127 and using flow cytometry. (H) Double-positive staining with pan-CD18 (anti-CD18 antibody-PE) and KIM127-FITC indicates activation of CD18 in normal and tumor tissues, including the breast, colon, lung, and liver. Nuclei (DAPI) were counterstained. Arrows indicate double-positive cells. All data are presented as the mean±SEM. n=3–5, *p<0.05, **p<0.01, ***p<0.001. TAMs, tumor-associated macrophages.

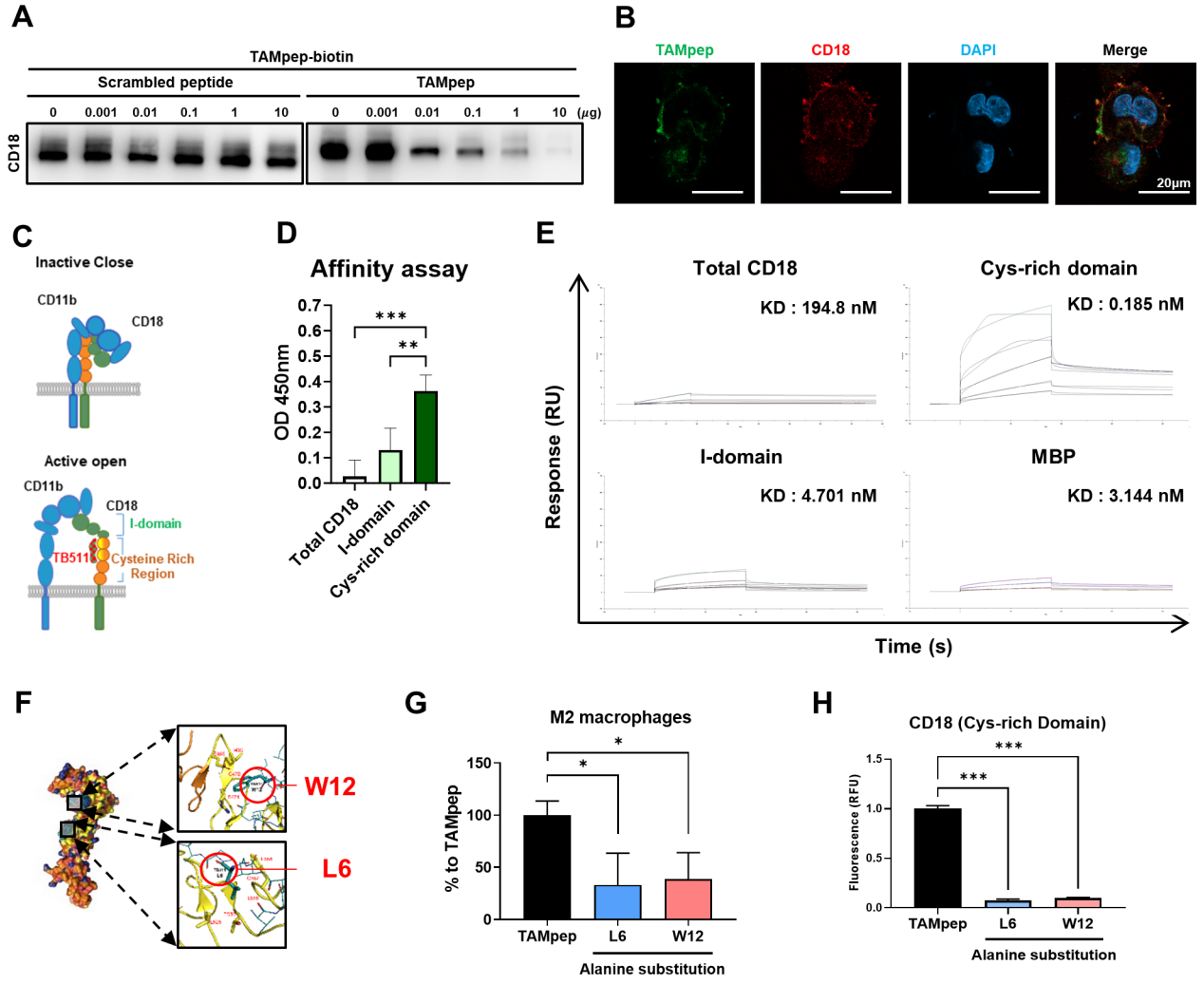

Figure 2 CD18 as a target protein of TB511 in M2-TAMs. (A) M2 macrophage lysates treated with scramble or TAMpep peptides (0–10 ug) were incubated with biotinylated TAMpep for 1 hour at RT. Biotinylated TAMpep-bound proteins were eluted by a pull-down assay, followed by measuring CD18 protein levels via western blotting. (B) Immunofluorescence staining showed the colocalization of TAMpep (green) and CD18 (red). Nuclei are counterstained with DAPI (blue); Scale bar, 20 µm. (C) Schematic diagram illustrating the inactive and active forms of the CD18 protein. (D) The affinity of total CD18, I-domain, and Cys-rich domain with TAMpep was evaluated by ELISA. (E) The binding kinetics of total CD18, I-domain, and Cys-rich domain with TAMpep were measured using a Biacore T-200. The equilibrium dissociation constant (K/D) was calculated. (F) Docking simulation of TB511 and CD18 (cysteine-rich region) by the CABS-dock server. (G) Assessment of FITC-TAMpep and alanine-substituted peptides binding to M2 macrophages or (H) to CD18 protein (Cys-rich domain) via flow cytometry or ELISA, respectively. The absorbance of each sample in the ELISA was determined using a fluorescence microplate reader and normalized to its intrinsic fluorescence value. All data are presented as the mean±SEM. *p<0.05, **p<0.01, ***p<0.001. AMs, tumor-associated macrophages.

domains of CD18: total CD18, I-domain, and cysteine (cys)-rich domain (figure 2C). As a result, TAMpep exhibited a high binding affinity to the cys-rich domain protein compared with I-domain and total CD18 proteins (figure 2D). In the SPR analysis, TAMpep showed higher affinity in the cys-rich domain (K_D:0.185 nM) compared with total CD18 (K_D:194.8 nM), I-domain (K_D:4.701 nM), and I-domain taq protein, MBP protein (K_D:3.144 nM). Notably, other proteins except cysteine-rich protein exhibited low RU values (<70) (figure 2E). We also predicted the binding sites of TAMpep to CD18 using peptide-protein modeling (CABS-dock server). While the binding of TAMpep to the total CD18 sequence of the bent (closed) form was not predicted, the leucine[6] residue of TAMPep binds to leucine (528), threonine (538), leucine (556), cysteine (557) and phenylalanine (558) of the cysteine-rich domain of the open form, and the tryptophan[12] residue predicted to bind to glutamic acid (466), isoleucine (469), cystein (470) and arginine (471) (figure 2F). To determine the binding site of TAMpep for CD18, we confirmed the binding affinity of the TAMpep, in which amino acids of L6 and W12 were substituted with alanine, on M2 macrophages and cys-rich domain protein. Peptides substituted with alanine showed a markedly reduced affinity to M2 macrophages and cys-rich domain protein (figure 2G,H). Therefore,

our results suggest that TAMpep of TB511 binds to the cysteine-rich domain of activated CD18, and in particular, Lys6 and Trp12 of TAMpep are the key binding residues.

TB511 targeting activated CD18 of M2 macrophages

To confirm whether TAMpep, the peptide carrier of TB511, preferentially attaches to M2 macrophages, TAMpep was synthesized by conjugation with FITC. TAMpep showed higher binding ability in M2 macrophages and TAMs compared with M0 and M1 type macrophages (figure 3A). TB511 comprised TAMpep and dKLA and showed cytotoxicity (IC50: 4.925 µM) against M2 macrophages, but TAMpep did not show cytotoxicity (figure 3B). To assess the impact of TB511 on apoptosis, we measured the activation of caspase 3 in each macrophage subtype using live-cell imaging. Activation of caspase 3/7 by TB511 was detected within 5 min and peaked at 15 min after incubation with TB511 in M2-TAMs. Although TB511 affected M2 macrophages, its effect was less pronounced. Notably, caspase 3/7 activation was not observed in M0 or M1 macrophages and was only mildly affected in M2 macrophages following TB511 treatment (figure 3C,D; online supplemental movie S1). Furthermore, the double positive expression of CD11b and TB511 in human tissues was significantly elevated in tumor tissues compared with normal tissues in the breast, lung, liver, kidney, and colon (figure 3E). To investigate whether TB511 selectively targets macrophages expressing activated CD18, we induced the activation of CD18 in T cells (Jurkat) and macrophages (THP-1) using Mn^{2+} and subsequently measured the cytotoxicity of TB511. The number of positive cells for the activated CD18 was higher in macrophages than in T cells when treated with Mn^{2+} (figure 3F). On treatment with TB511, the number of apoptotic cells significantly increased in activated macrophages, whereas the number of apoptotic cells in activated T cells remained unchanged compared with inactivated cells (figure 3G). Moreover, TB511 induced more apoptosis in macrophages than in other immune cells such as T cells, NK cells, dendritic cells, and neutrophils obtained from the spleen of mouse (figure 3H). Therefore, these results suggest that TB511 induces apoptosis by primarily targeting M2-TAMs, which exhibit high expression levels of activated CD18.

Endocytosis and endosome escape of TB511 into M2 macrophages

Recently, the elucidation of mechanisms of action for the cytoplasmic delivery efficiency of drugs using cell-penetrating molecules and endosomal escape has emerged as a significant area of research.[30] To monitor the dynamics of the cell membrane and intracellular transport of TB511 in M2 macrophages, we conjugated TB511 (TB511-AuNRs) with carboxylic acid-functionalized gold nanorods. These were then tracked using astigmatism imaging and polarized light-sheet illumination, allowing us to resolve the 3D spatial trajectory and rotational behavior of TB511-AuNRs in M2 macrophages. Differential interference contrast and super-resolution radial fluctuations images revealed the intracellular distribution of mitochondria (green) and nuclei (blue) in M2 macrophages (figure 4A). On contact with the cell membrane, the lateral movements and rotations of TB511-AuNRS were limited due to the viscosity of the cell membrane and the interaction between them.[31] The gradual loss of displacements in x, y, and z directions, along with scattering intensity fluctuations, indicated the binding of TB511-AuNRs to the receptors on the cell membrane (figure 4B,C). At certain times, TB511-AuNRs exhibited reduced spatial movement and slow orientation changes, suggesting that TB511-AuNRs were enveloped by the cell membrane to assemble the endocytic machinery.[32] Following these quiet periods, noticeable spatial movement in the x, y, and z directions was observed, indicating that the TB511-AuNRs were detached from the membrane and transported intracellularly. The representative rotational angles and corresponding scattering images of TB511-AuNRs in M2 macrophages provide insight into the rotational states of TB511-AuNRs during their internalization processes (figure 4D; online supplemental movie S2). To investigate the cellular uptake of TB511, M2 macrophages were treated with endocytosis inhibitors: chlorpromazine (CPZ) to inhibit clathrin-mediated endocytosis (CME), methyl-β-cyclodextrin (MβCD) to inhibit caveolae-mediated endocytosis, and cytochalasin D (CyD) to inhibit macropinocytosis (MP). Both CPZ and CyD, but not MβCD, inhibited TB511 uptake, thereby decreasing TB511-induced apoptosis (figure 4E,F). Additionally, M2 macrophages were treated with bafilomycin A1 (Baf-A1) and chloroquine (CQ) to inhibit the acidification of early endosomes and prevent the maturation and fusion of endosomes and lysosomes. Subsequently, we evaluated the colocalization of early endosome antigen 1 (EEA1) and TB511-Cy5 in endosomes. Treatment with Baf-A1 and CQ increased the colocalization of EEA1 and TB511-Cy5 in endosomes and significantly decreased TB511-induced apoptosis (figure 4G,H). Therefore, these results suggest that TB511 is internalized into cells via CME and micropinocytosis and subsequently exits from the endosomes into the cytoplasm.

Abrogation of the antitumoral effect of TB511 by CD18 deficiency

To determine whether TB511 induces apoptosis in M2 macrophages through CD18, we inhibited CD18 expression in M2 macrophages using CD18/sgRNA in cas9 stable THP-1 cells and anti-CD18 antibody. Consequently, the cytotoxicity of TB511 was significantly diminished in CD18/sgRNA-transfected cells compared with mock-transfected cells (online supplemental figure 4A,B). Furthermore, blocking of CD18 using antibodies attenuated TB511-induced apoptosis in M2 macrophages, accompanied by a downregulation in the gene expression of caspase 3, 8, and 9 (online supplemental figure 4C,D). We also found that the colocalization of TB511 with

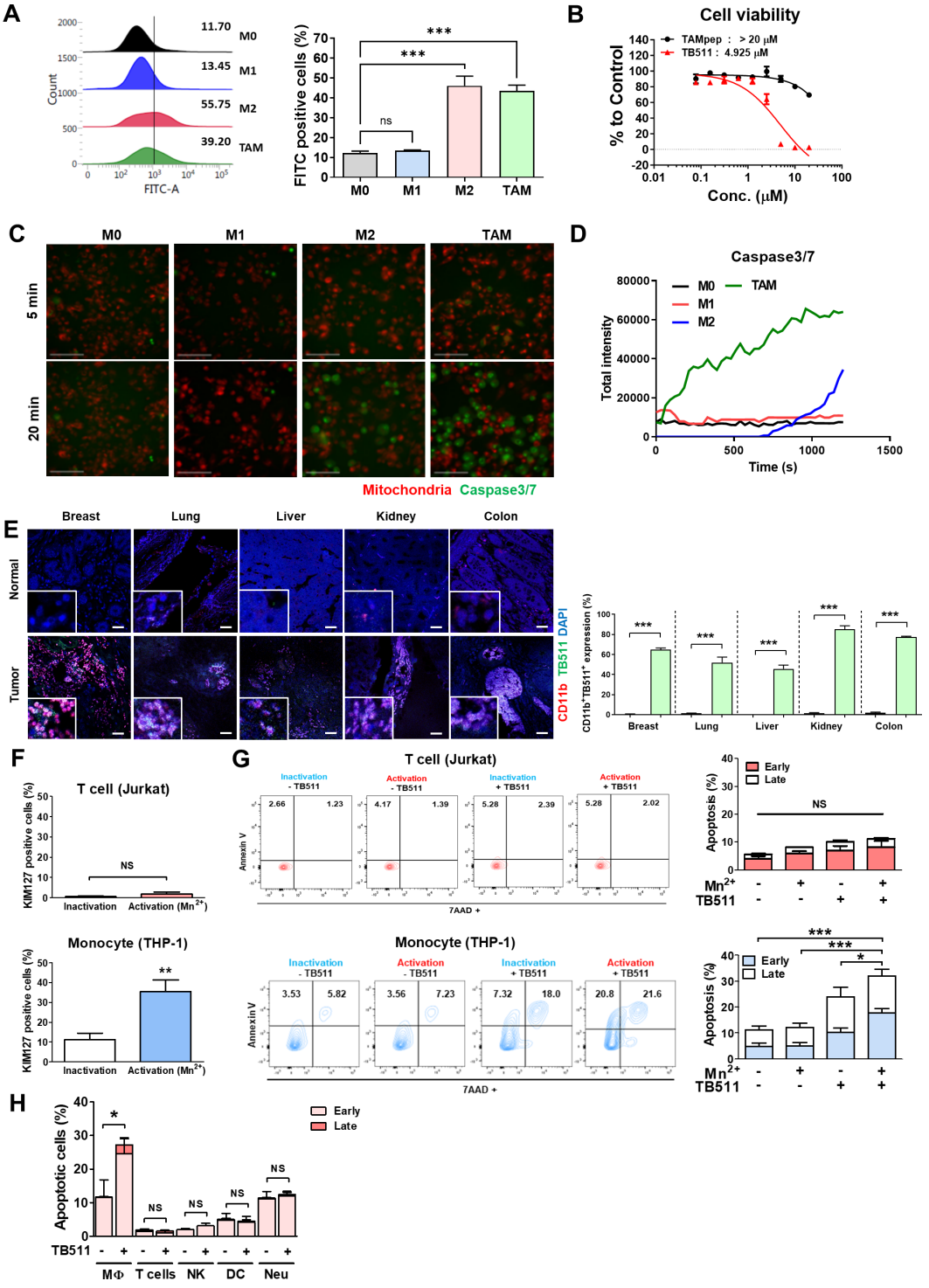

Figure 3 TB511 targeting activated CD18 of M2 macrophages. (A) THP-1 cells were differentiated into MO, M1, or M2 macrophages. Cells were treated with FITC-conjugated TAMpep. The affinity of TAMpep and cells was measured using flow cytometry. (B) The M2 macrophages were treated with TAMpep or TB511 by concentration from 0.01 uM to 20 uM. Cell viability was measured by CCK-8 assays. All data are presented as the mean±SEM. n=4 ***p<0.001. (C, D) Activation of caspase 3/7 (green) was observed using live-cell imaging fluorescence microscopy. The mitochondria were counterstained with MitoTracker (red). The total intensity of the area is graphed. (E) The colocalization of TB511 (yellow) with CD11b+cells (green) was assessed via confocal microscopy in both normal and tumor tissues, including those from breast, lung, liver, kidney, and prostate. Scale bar, 100 µm. (F) Jurkat or THP-1 cells were treated with 1 mM $Mn2^{+}$ for 1 hour at 37°C. The degree of activated CD18 in cells was stained with mAb KIM127 and analyzed using flow cytometry. (G) Activated Jurkat or THP-1 cells were treated with TB511 (1 uM) for 1 hour. Cell viability was measured by flow cytometry using Annexin V (APC) and 7AAD staining. (H) Macrophages (F4/80+cells), T cells (CD3+cells), NK (NKp46+cells), dendritic cells (CD11c+cells), and neutrophils (Gr-1+cells) were treated with 1 µM TB511. The cell death was measured by Annexin V staining and was analyzed using flow cytometry. All data are presented as the mean±SEM. n=3–5, *p<0.05, **p<0.01, ***p<0.001.

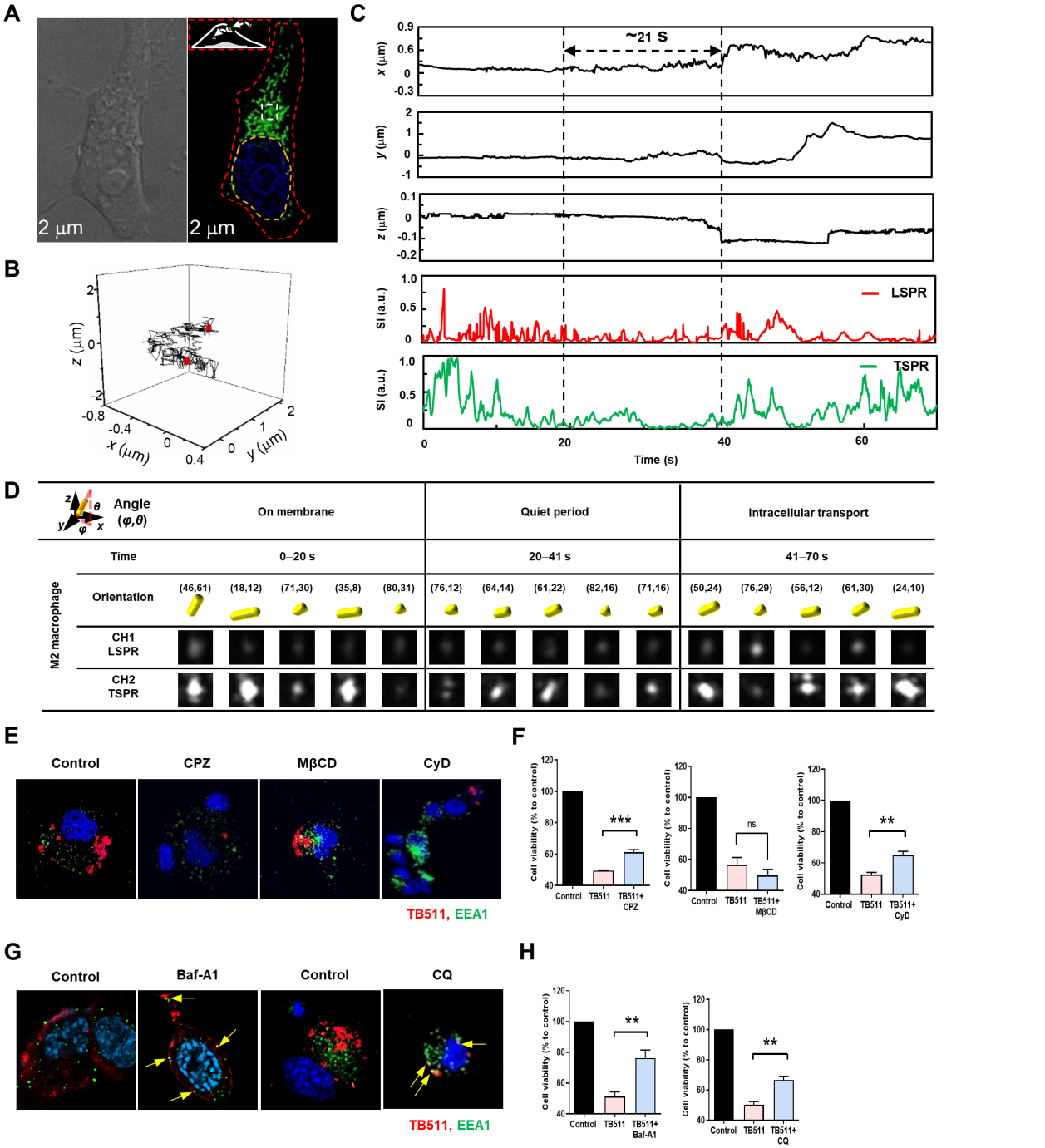

Figure 4 Endocytosis and endosome escape of TB511 into M2 macrophages. (A) DIC and fluorescence-based SRRF images of M2-differentiated THP-1 macrophages stained with mitochondria (green) and nuclei (blue), with TB511-AuNRs endocytosis occurring in the white frame. Red and yellow dotted lines indicate the contours of the cell and nucleus, respectively. (B) 3D tracking trajectory of TB511-AuNRs in the same region (white frame in (A)) of live single M2 macrophages using *i*MLSM. The circular dot denotes the starting point, and the red triangle denotes the movement endpoint. (C) Corresponding displacements of TB511-AuNRs in the x, y, and z-directions. Description of different rotational states of single TB511-AuNRs on the upper surface of live single M2 macrophages using *i*MLSM. (D) Description of the rotational angle and corresponding scattering image of TB511-AuNRs in M2 macrophages. (E) M2 macrophages were pretreated with CPZ, CyD, and MβCD, followed by TB511-Cy5 (20 μM) treatment and anti-EEA 1 antibody staining, revealing TB511 (red) and endosomes (green) colocalization. (F) M2 macrophages treated with CPZ, CyD, and MβCD, followed by TB511 (1 μM), underwent CCK8 assays to assess cell viability. (G) M2 macrophages, pretreated with Baf-A1 or CQ, were treated with TB511-Cy5 and stained with anti-EEA 1 antibody. Colocalization of TB511-Cy5 (red) and endosomes (green) was observed using confocal microscopy. (H) M2 macrophages pretreated with Baf-A1 or CQ were treated with TB511 (1 μM) for 1 hour. Apoptosis of cells induced by TB511 was measured using CCK8 assays. All data are shown as the mean±SEM. n=3, **p<0.01, ***p<0.001. DIC, differential interference contrast; *i*MLSM, integrated multidimensional light-sheet microscopy; LSPR, longitudinal surface plasmon resonance; SRRF, super-resolution radial fluctuations; TSPR, transverse surface plasmon resonance.

mitochondria, including the dKLA peptide that binds to mitochondrial membranes to induce cell death, was inhibited by anti-CD18 antibodies (online supplemental figure 4E). Moreover, antibody-mediated blockade of CD18 reduced TB511-induced expression of cytochrome c and caspase 3 in M2 macrophages (online supplemental figure 4F,G). To verify whether TB511 exerts its antitumor effect via CD18 of TAMs, we examined the efficacy of TB511 using CD18-deficient mice. As a result, the cytotoxicity of TB511 was diminished in bone marrow-derived macrophages obtained from CD18-KO mice, and the expression of cleaved-caspase 3 was also suppressed (figure 5A,B). In CRC model, TB511 significantly reduced the tumor size in WT mice, but these effects were not observed in CD18-KO mice (figure 5C). The number of M2-TAMs (F4/80$^+$ CD206$^+$/CD45$^+$ cells) significantly decreased in WT tissues, whereas the populations of M2-TAMs (F4/80$^+$ CD206$^+$/CD45$^+$ cells) did not change in response to TB511 in CD18-KO mice (figure 5D). In non-small cell lung cancer (NSCLC) model, the antitumoral effects of TB511 were only evident in the WT mice and not in CD18-KO mice (figure 5E). Like the results in CRC mouse model, M2-TAMs were reduced by TB5111 only in WT mice, with no change observed in CD18 KO mice (figure 5F). Based on these findings, we suggest that CD18 plays a crucial role in the action of TB511 for targeting M2 TAMs in TME of CRC and NSCLC and may be a potent target protein for cancer treatment.

Antitumor effect of TB511 by targeting M2-TAMs in the mouse model

To determine whether elimination of M2-TAMs by TB511 results in antitumor effects in solid cancer mouse models, we assessed the efficacy of TB511 in an orthotopic CRC and subcutaneous NSCLC mouse model. TB511 markedly suppressed tumor growth in CRC mouse models and reduced the PCNA-positive cells in tumor tissues (figure 6A–C). Furthermore, the number of M2-TAMs (CD206$^+$F4/80$^+$CD45$^+$ cells) was significantly reduced in the TB511 group compared with the control group, leading to a significant increase in the M1/M2 ratio in the TB511 group (figure 6D). Additionally, the CD18-positive cells were significantly reduced by TB511 treatment in tumor tissues (figure 6E). To identify the changes of TME by TB511, we measured CD8$^+$ T cells and inflammatory factors in tumor tissue. In CRC tissues, the number of CD8$^+$ T and Granzyme B$^+$ cells significantly increased following TB511 treatment (figure 6F). Next, we evaluated the anticancer effects of TB511 in NSCLC. As a result, the tumor growth was significantly suppressed by TB511 (figure 6G). The PCNA-positive cells were significantly reduced in TB511-treated tumor tissues (figure 6H). Moreover, TB511 treatment significantly increased the number of M1 macrophages while reducing M2 macrophages, leading to elevated M1/M2 ratio in the TB511-treated group (figure 6I). The CD18-positive cells were reduced in TB511-treated tumor tissues (figure 6J). Using FACs analysis, we confirmed that the population of CD8$^+$ T cells was increased while decreasing exhausted CD8$^+$ PD-1$^+$ T cells in the TB511-treated group (figure 6K). Additionally, TB511 suppressed tumor growth in TNBC and RCC mouse models (online supplemental figure 5A,B). Gene expression of M2 markers was significantly reduced by TB511, but M1 markers were not altered (online supplemental figure 6A–D). Therefore, these results suggest that TB511 selectively eliminates M2-TAMs in the TME, leading to reprogramming into an anti-tumoral TME by infiltrating CD8$^+$ T cells.

We also assessed the impact of TB511 on tissue-resident macrophages in normal tissues, including the brain, skin, kidney, and liver. TB511 reduced the number of CD206$^+$ M2-TAMs in CRC mouse tumor tissues but did not affect the number of CD86$^+$ M1-TAMs or the population of F4/80$^+$ tissue-resident macrophages in the brain, skin, kidneys, and liver of the mice (figure 6L). Therefore, these results suggest that TB511 selectively eliminates M2-TAMs in the TME, leading to reprogramming into an antitumoral TME by infiltrating CD8$^+$ T cells.

Antitumor effect of TB511 by targeting M2-TAMs in a NSCLC humanized mice model

To assess the clinical feasibility of TB511, we used a humanized mouse model. Immunodeficient mice (SID mice) were engrafted with human CD34$^+$ stem cells; the antitumor effect of TB511 was then assessed according to the study schedule. In immunodeficient mice, the antitumor effect of TB511 completely disappeared, suggesting that an intact immune system is indispensable for eliciting TB511 activity (online supplemental figure 7). However, in the humanized lung cancer mouse model, profound anticancer effects were observed following TB511 treatment (figure 7A). Tumor-infiltrating immune cell populations were also significantly altered by TB511; we observed an increased number of M1-TAMs (CD206$^+$CD11b$^+$/CD45$^+$ cells) and decreased number of M2-TAMs (CD86$^+$CD11b$^+$/CD45$^+$ cells) in the TB511-treated groups (figure 7B). In addition, the CD86-positive M1 macrophages and CD206-positive M2 macrophages were increased in humanized lung cancer mouse tissue treated with TB511 (figure 7C). We also examined changes in CD18$^+$ macrophages following TB511 treatment. The population of CD18-positive cells was significantly reduced in the TB511-treated group. Consequently, the KIM127$^+$CD11b$^+$ macrophages, indicative of CD18 activation, were significantly decreased in TB511-treated humanized mouse tumor tissues (figure 7D,E). Furthermore, we investigated the changes in CD8$^+$ T cells induced by TB511 in tumor tissues. The CD8-positive cells were significantly increased in the TB511-treated group (figure 7F). Granzyme B-positive CD8$^+$ T cells significantly infiltrated the TME, while the exhausted CD8$^+$ T-cell population (PD-1 CD88$^+$/CD45$^+$ cells) was diminished in the TB511-treatment groups (figure 7G–I). In addition, the NCAM-1$^+$ NK cells in TB511-treated tumor tissues were significantly increased (figure 7J). Thus, these findings suggest that TB511 exerts antitumor

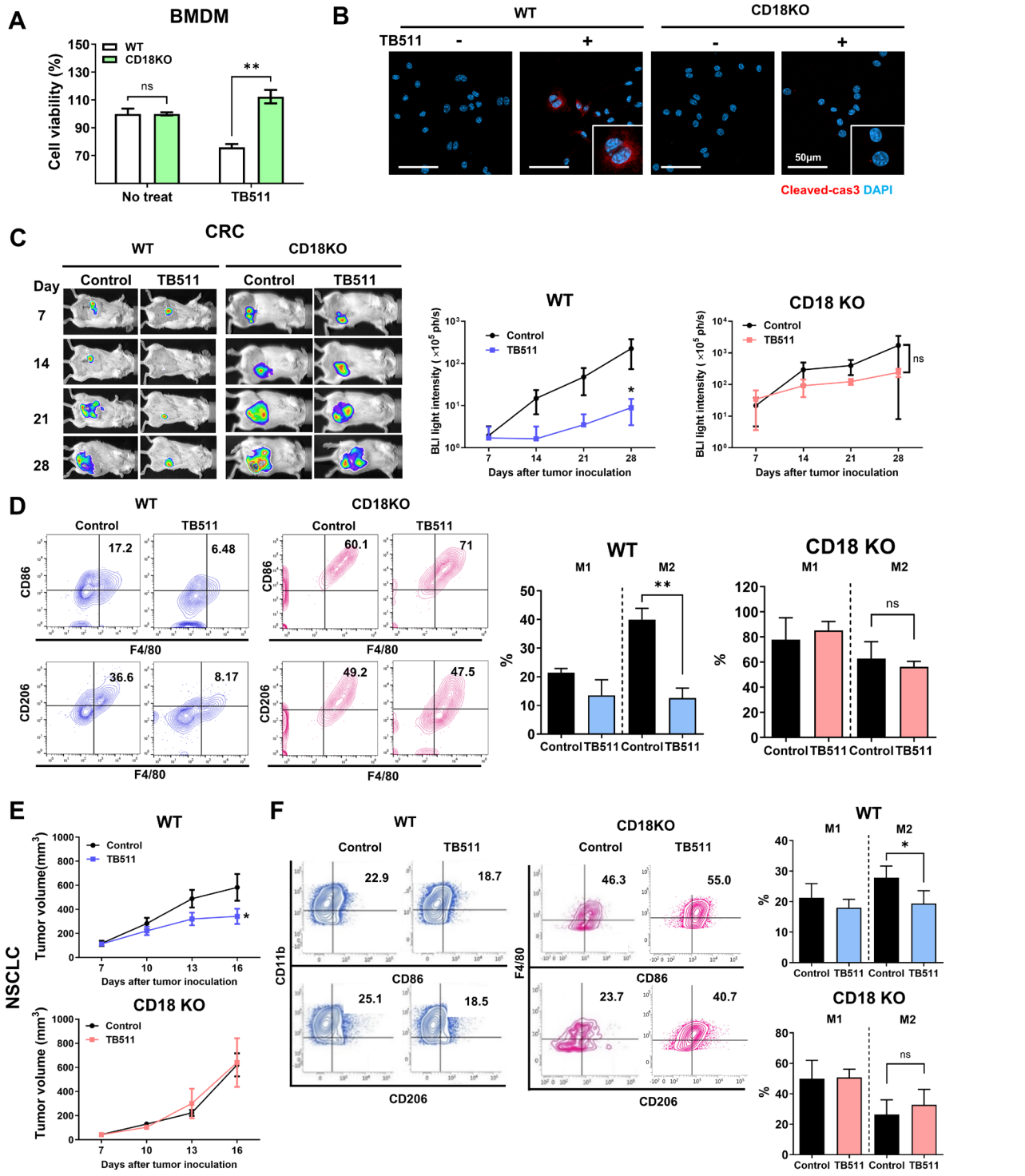

Figure 5 Abrogation of the antitumoral effect of TB511 by CD18 deficiency. (A) bone marrow-derived monocytes from BALB/c (WT) and CD18 knockout mice (CD18KO) were cultured for 5 days for BMDM differentiation, treated with 2.5 µM TB511 for 24 hours, and assessed for cell viability using MTS assay. (B) Activation of cleaved-cas9 (red) in WT or CD18KO BMDMs treated with TB511 (2.5 µM) was observed by confocal microscopy. (C) In vivo imaging of WT or CD18KO colorectal cancer mouse model. (D) Bioluminescence of tumor in the WT and CD18KO mouse models was quantified and graphed. n=5 (WT group) or n=3 (CD18 KO group). (E) M1-TAMs and M2-TAMs in tumor tissues of WT mice presented as $F4/80^+CD86^+$ and $F4/80^+CD206^+$ in gating $CD45^+$ cells using flow cytometry. In tumor tissues of CD18KO mice, M1-TAMs or M2-TAMs are represented as $F4/80^+CD86^+$ or $F4/80^+CD206^+$ gated on $CD45^+$ cells using flow cytometry. (F) WT or CD18KO mice were inoculated with LLC cells for establishment of lung cancer mouse model and were treated with TB511, and tumor volume was measured. n=10 (WT mice) or n=4 (CD18KO mice). (G) M1-TAMs and M2-TAMs in tumor tissues of WT mice presented as $CD11b^+CD86^+$ and $CD11b^+CD206^+$ in gating $CD45^+$ cells using flow cytometry. M1-TAMs or M2-TAMs are represented as $F4/80^+CD86^+$ or $F4/80^+CD206^+$ gated on $CD45^+$ cells using flow cytometry in tumor tissues of CD18KO mice. All data are presented as mean±SEMs. *p<0.05, **p<0.01. TAMs, tumor-associated macrophages; WT, wild-type.

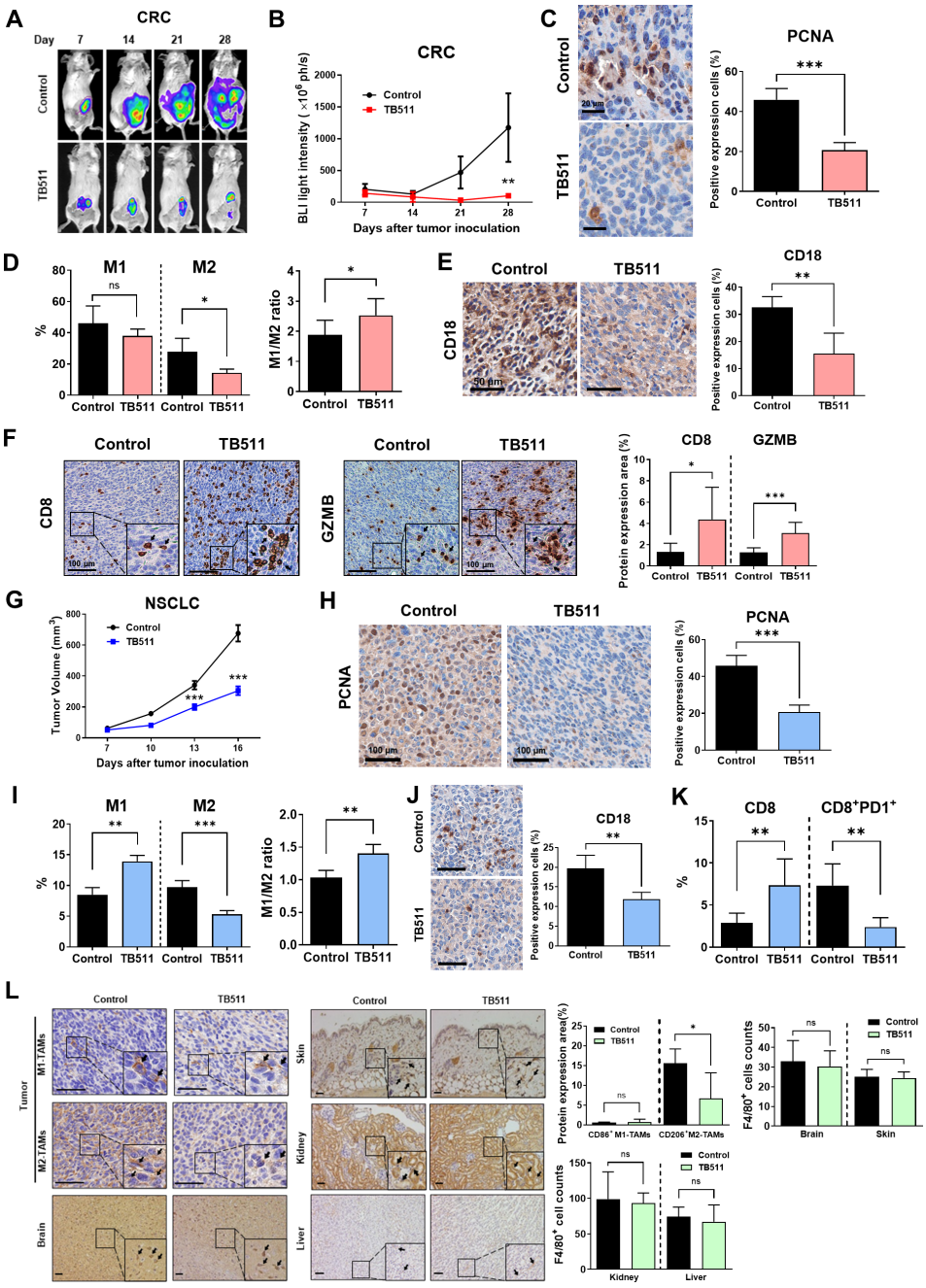

Figure 6 Antitumor effect of TB511 by targeting M2-TAMs in the mouse model. (A, B) Orthotopic models for CRC used CT26 Luc cells. The d-Luciferin (3 mg/mouse) was intraperitoneally injected, and tumor growth was quantified by in vivo imaging system. Mice were subcutaneously treated with 200 nmol/kg TB511 every 3 days. (n=12). (C) The PCNA-positive cells were measured in tumor tissues by IHC. (D) In colorectal cancer tissue, M1-TAMs or M2-TAMs were stained as F4/80$^+$CD86$^+$ cells or F4/80$^+$CD206$^+$ (bottom panel) gated on CD45$^+$CD11b$^+$ cells, and the M1/M2 ratio was calculated (n=4). (E) The CD18-positive cells were measured in tumor tissues by IHC. (F) CD8$^+$ T cells and activation of granzyme B (GrB) in colorectal tumor specimens were observed by immunohistochemistry staining. Scale bar, 50 µm. (n=7). All data are presented as the mean±SEM *p<0.05, **p<0.01, ***p<0.001. (G) Subcutaneous tumor mouse models for NSCLC were established with LLC cells. Mice were subcutaneously treated with 200 nmol/kg TB511 every 3 days. Tumor size was measured using a digital caliper (n=12). (H) The PCNA-positive cells were measured in tumor tissues by IHC. (I) In lung cancer tissue, M1-TAMs or M2-TAMs were stained as F4/80$^+$CD86$^+$ cells or F4/80$^+$CD206$^+$ (bottom panel) gated on CD45$^+$ cells, and the M1/M2 ratio was calculated (n=5). (J) The CD18-positive cells were measured in tumor tissues by IHC. (K) Infiltrated CD8$^+$ T cells (CD45$^+$CD8$^+$ gated on CD45$^+$ cells) and the exhausted CD8$^+$ T cells (CD8$^+$PD-1$^+$ gated on CD45$^+$ cells) were measured using flow cytometry in lung cancer tissue. (L) Macrophages in both tumor and normal tissues of the mice were stained using immunohistochemistry. M1-TAMs were marked as CD86$^+$, M2-TAMs were stained as CD206,$^+$ and tissue-resident macrophages, including the brain, skin, kidney, and liver, were labeled as F4/80$^+$. Scale bar, 50 µm. Macrophage quantification is graphically represented. n=6 (tumor tissue) or n=3 (normal tissue). All data are presented as the mean±SEM. *p<0.05, **p<0.01, ***p<0.001. CRC, colorectal cancer; IHC, immunohistochemistry; TAMs, tumor-associated macrophages.

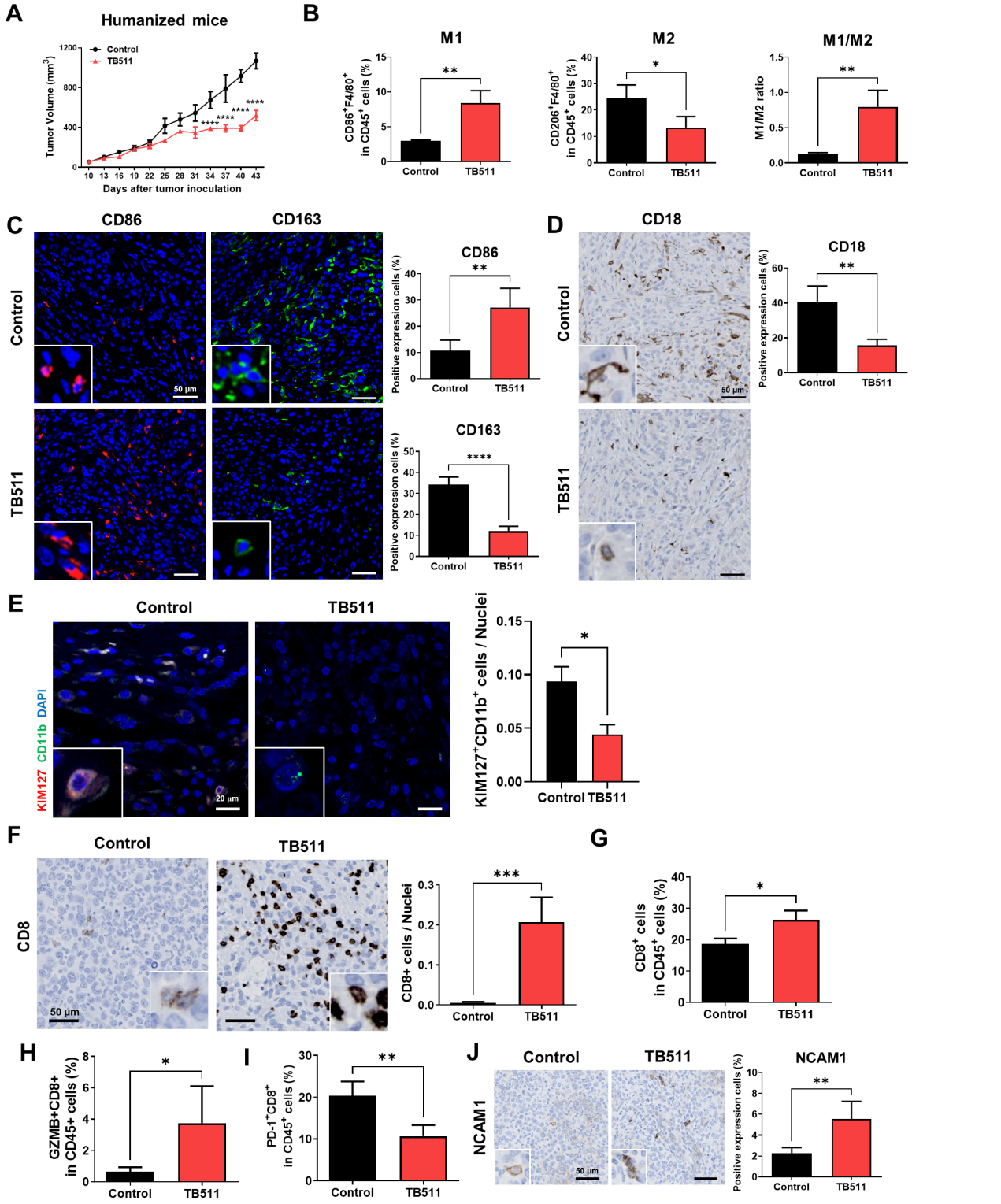

Figure 7 Antitumor effect of TB511 by targeting M2-TAMs in a NSCLC humanized mice model. (A) Humanized mice inoculated with A549 cells were treated every 3 days with PBS (control) and TB511. Tumor growth was measured every 3 days and plotted as a line graph. (B) Macrophages in the tumor tissue of each group were measured by flow cytometry. The M1-TAMs and M2-TAMs were stained with $CD11b^+CD86^+$ or $CD11b^+CD206^+$ gated on $CD45^+$, respectively. The M1/M2 ratio was calculated based on the percentages of M1-TAMs and M2-TAMs. The $CD86^+$, $CD206^+$, and $CD18^+$ cells were measured in humanized tumor tissues by IHC. (F) $CD8^+$ cells in humanized NSCLC tumor tissues from each group as determined by IHC. Scale bar, 50 μm. (G–I) The percentages of infiltrated ($CD8^+$ gated on $CD45^+$ cells), activated $CD8^+$ T cells ($CD8^+$ granzyme B^+ gated on $CD45^+$ cells), and exhausted $CD8^+$ T cells ($CD8^+PD\text{-}1^+$ gated on $CD45^+$ cells) in tumor tissues were measured by flow cytometry. (J) $NCAM1^+$ cells in humanized NSCLC tumor tissues from each group as determined by immunohistochemical staining. Scale bar, 50 μm. Values are presented as mean±SEMs. *p<0.05, **p<0.01, ***p<0.001, ****p<0.0001. IHC, immunohistochemistry; NSCLC, non-small cell lung cancer; TAMs, tumor-associated macrophages.

effects by targeting M2-TAMs through activated CD18 in a humanized mouse model, highlighting its potential for clinical application.

Antitumor effect of TB511 by targeting M2-TAMs in humanized pancreatic cancer mice model

Next, we evaluated the anticancer efficacy of TB511 and its impact on immune cells in a humanized mouse model of pancreatic cancer. TB511 significantly inhibited tumor growth and reduced Ki67 expression in tumor tissues (figure 8A,B). Furthermore, we assessed the effects of TB511 on epithelial-mesenchymal transition (EMT), a key indicator of tumor progression. TB511 treatment led to a significant upregulation of E-cadherin (epithelial cell marker) and a downregulation of vimentin (mesenchymal marker), suggesting a suppression of EMT (figure 8C). To determine whether TB511 reduces M2 macrophages within the TME, tumor tissues were analyzed using IHC. The TB511 groups exhibited a significant reduction in CD163-expressing cells, a marker of M2 macrophages (figure 8D), as well as a marked decrease in activated $CD18^+$ macrophages ($KIM127^+CD11b^+$ cells) (figure 8E and online supplemental figure 8A). $CD8^+$ T cells were significantly increased in TB511-treated tumor tissues (figure 8F). However, the TB511 group has no effect in KIM127-positive cells of macrophages and CD8 T cells compared with the PBS group in normal tissues such as spleen, liver, lung, and brain (online supplemental figure 8B,C). To investigate the effect of TB511 on immune cells in the TME, tumor tissues were analyzed using spatial transcriptomics. In the PBS group, tissue cells contributing to tumor formation were distributed into five distinct clusters: epithelial cells, endothelial cells, stromal cells, fibroblasts, and neural cells. However, in the TB511 group, the stromal cell cluster was absent, resulting in a reduction to four clusters compared with the PBS group (online supplemental figure 9A). As shown in figure 8G, the distribution of cells in the PBS and TB511 groups was visualized and analyzed using UMAP. The proportion of immune cells was 18% in the PBS group and 23% in the TB511-treated group, indicating a higher immune cell population in the TB511-treated group (figure 8G). When analyzing these immune cells, in the TB511 group, the gene cluster of M1 macrophages increased, while the gene cluster of M2 macrophages decreased. There was an increase in CD8 T cells and NK cells. Treg cells were not observed in TB511 groups (figure 8G and online supplemental figure 9B). Additionally, we compared the expression levels of ITGB2 among different cell types within the tumor tissue. We found that ITGB2 expression was low in non-immune cells, including epithelial, endothelial, stromal, and fibroblast cells. Among immune cells, ITGB2 expression was highest in M2 macrophages. Furthermore, TB511 treatment resulted in a reduction of ITGB2 expression in M2 macrophages (online supplemental figure 9C).

To investigate whether the reduction of M2 macrophages by TB511 leads to $CD8^+$ T cell activation, we analyzed the composition of immune cells around CD8 T cells and the gene expression levels of exhaustion markers (PDCD1, CTLA4, FOXP3, and LAG3) and activation markers (GZMB and IFNG). In the PBS group, CD8 T cells were located close to M2 macrophages (blue green), and the number of cells expressing exhaustion marker genes (CTLA4, FOXP3, and LAG3) increased. On the other hand, CD8 T cells in the TB511 group were located near dendritic cells (light pink) and NK cells (green), and the expression of activation marker genes (GZMB and IFNG) increased (figure 8H and online supplemental figure 10). Therefore, these findings suggest that TB511 exerts its anticancer effects by targeting M2-TAMs expressing activated CD18 within the TME of human pancreatic cancer, thereby inducing CD8 T cell activation and promoting immune responses.

DISCUSSION

CD18, an integrin β2 subunit predominantly expressed in leucocytes, including macrophages, plays a pivotal role in cell adhesion and migration.[33] A negative correlation has been observed between CD18 expression and patient survival.[13 15] Interestingly, another study revealed a strong correlation between CD18 overexpression and significant infiltration of M2 macrophages, as compared with other lymphocytes, in ovarian cancer tissue.[14] In this study, we observed a significant increase in CD18 expression in M2-TAMs among various macrophage subtypes. Additionally, we demonstrated a significant increase in CD18 expression in various tumor tissues, including breast, colon, lung, and liver, and found a significant correlation with MRC1, a marker for M2 macrophages. The high expression of CD18 suggests its potential as a target for anti-cancer therapy. Furthermore, TB511, which binds to CD18, shows promise as an immunotherapeutic agent targeting M2 TAMs.

The CD18 protein domain, which includes the I-domain, cysteine-rich region, and a tail domain, plays a pivotal role in leucocyte adhesion, signaling, and potentially disease processes.[29 34] The extracellular domain of CD18, which encompasses the I-domain and cysteine-rich protein, is essential for ligand binding and integrin function. This domain undergoes substantial conformational changes, transitioning the receptor from an inactive to an active state.[29] Our study revealed that TB511, which binds to CD18, showed higher binding to cysteine-rich protein than to the I-domain among the extracellular domains. However, TB511 does not bind to the total CD18 protein, which contains cysteine-rich proteins, indicating differences depending on the closed form structure. Thus, activated CD18 emerges as an important target protein.

CD18 activation, especially in macrophages and T cells, is a critical aspect of various immune functions and is influenced by various factors, including cytokines, chemokines, and ions.[11 35] Among ions, manganese (Mn^{2+}) plays a key role in CD18 activation by shifting integrins into high-affinity conformation through integrin outside-in

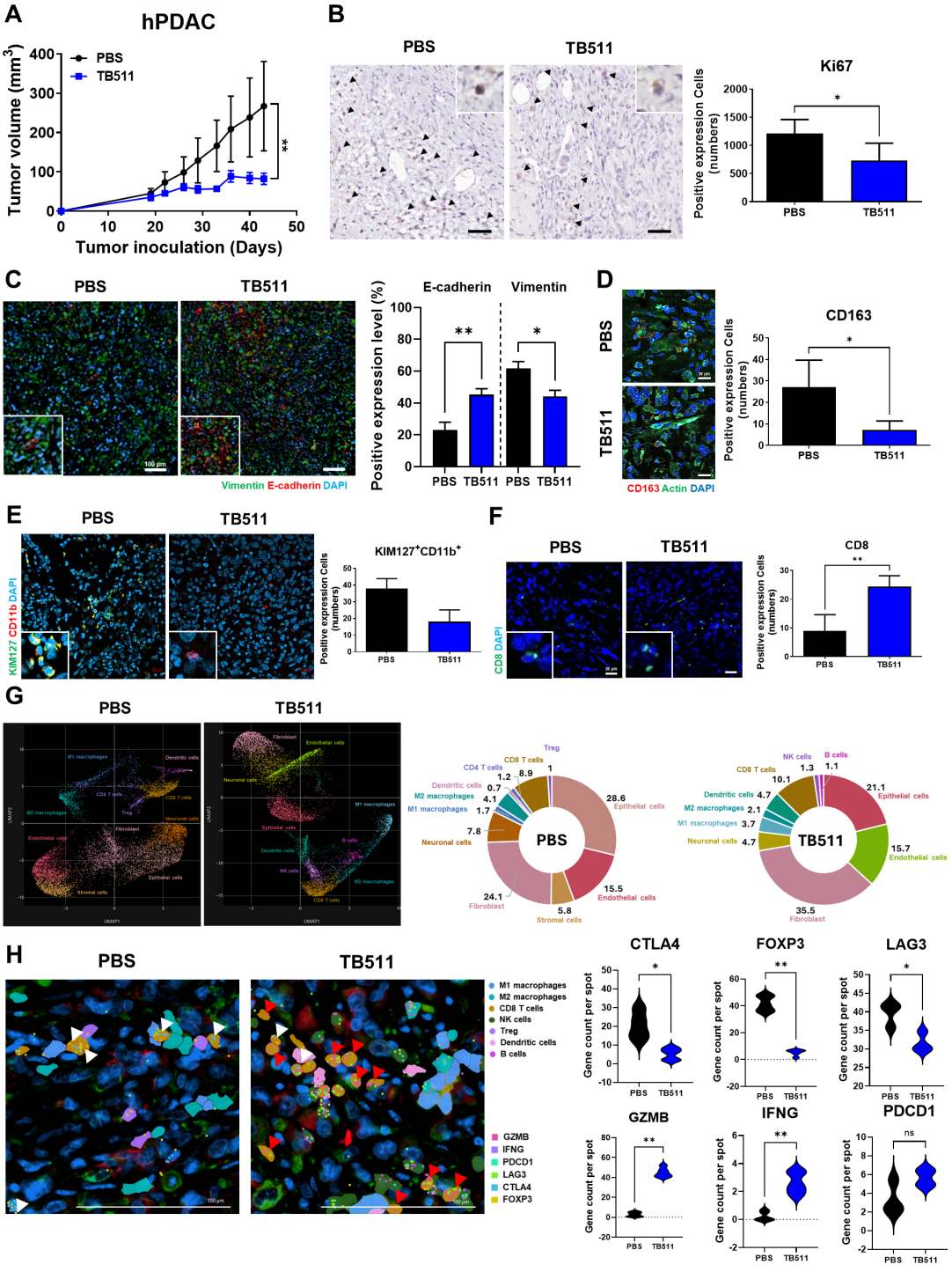

Figure 8 Antitumor effect of TB511 by targeting M2-TAMs in humanized pancreatic cancer mice model. Humanized mice inoculated with PANC1 cells were treated twice a week with PBS (control) and TB511. (A) Tumor growth curve in mouse model. After subcutaneous implantation, tumor volume was measured twice a week in mm^3 (n=4 per group). (B) Representative images are IHC staining of Ki67 in tumor tissues (left). The graph quantified Ki67 positive cells (right). Scale bar: 50 µm. (C) Representative images are immunofluorescence staining of E-cadherin and vimentin in tumor tissues (left). Scale bar: 100 µm. The graph analyzed the area of positive cells (right). (D) Representative images are immunofluorescence staining of CD163 and actin in tumor tissues (left). The graph quantified CD163 positive cells (right). Scale bar: 20 µm. (E) Representative images are immunofluorescence staining of KIM127 and CD11b in tumor tissues (left). The graph quantified KIM127 and CD11b positive cells (right). Scale bar: 20 µm. (F) Representative images are Immunofluorescence staining of CD8 in tumor tissues. Scale bar: 20 µm. Scale bar: 20 µm. (G) A representative image showing cell clusters within the tumor tissue. The genes in tumor tissues were analyzed using spatial transcriptomics. The cell clusters were analyzed using UMAP. (H) Representative images of exhausted genes (white arrow) and activation factor genes (red arrow) of CD8 T cells in tumor tissues. Scale bar: 100 µm. The graph analyzed the expression levels of genes such as CTLA4, FOXP3, LAG3, GZMB, IFNG, and PDCD1. All data are represented as the means±SEM; *p<0.05, **p<0.01, ns=no significant.

signaling in immune cells.[36] Interestingly, while CD18 activation in T cells is involved in antigen-dependent activation, its expression level is relatively low compared with other leucocytes.[35 37] Conversely, macrophages express CD18 at a higher level, significantly contributing to leucocyte migration and retention during the progression of a staged immune response.[29 38] In this study, we found that Mn^{2+} induced CD18 activation in macrophages, leading to high cytotoxicity of TB511. However, in T cells, CD18 activation by Mn^{2+} had no effect, and no cytotoxicity by TB511 was observed. Recently, manganese has been implicated in tumor progression and metastasis, with evidence showing its accumulation within primary tumors in the LLC model, while its concentration is reduced in peripheral blood.[39] Our results found that M2 macrophages and TAMs exhibited higher CD18 activation compared with other macrophage subtypes as well as other immune cells. Significantly, Usami *et al* found that CD11b/CD18 of macrophages induced macrophage infiltration into the tumor nest and TAM-derived protumor function.[40] Accordingly, our data confirmed that activated CD18 was highly expressed in tumor tissue compared with normal tissue. TB511 appeared to specifically bind CD11b cells in tumor tissues, particularly reducing M2 TAMs, but had no effect on M1 macrophages or resident macrophages in normal tissues. In a humanized cancer mouse model, TB511 was shown to target the M2-TAMs expressing activated CD18.

Targeting CD18 has recently been recognized as a potential therapeutic strategy in oncology. Numerous studies have identified CD18 as a potent prognostic biomarker across various cancer types.[14 41 42] Recent advancements in structural surface omics have revealed an Acute Myeloid Leukemia-specific conformation of integrin β2, making it a potential target for CAR T cell therapy.[43] Additionally, inhibiting Mac-1 (CD11b/CD18) has been found to enhance tumor responsiveness to radiation by reducing the recruitment of myeloid cells.[44] Surprisingly, despite these findings, no previous studies have explored the targeting of M2 TAMs expressing activated CD18 within the TME. In this study, we demonstrate that TB511 attenuated the cytotoxicity of M2 TAMs by blocking CD18. This effect was further validated by the abolition of anticancer effects of TB511 in CD18 knockout mice. These findings highlight the dual role of CD18 not only as a cancer biomarker but also as a viable target for anticancer therapy, while suggesting the potential of TB511 as the first anti-cancer drug targeting CD18 on M2 TAMs.

PDCs represent a promising strategy for targeted cancer therapy, offering advantages such as enhanced cellular permeability and improved drug selectivity.[45] In the development of these targeted drug delivery systems, the processes of endosomal escape and internalization are of paramount importance.[46] Internalization, or endocytosis, encompasses several mechanisms, including caveolae-mediated endocytosis, micropinocytosis, receptor-mediated endocytosis, and phagocytosis. These processes enable cells to absorb extracellular molecules, playing a critical role in the selective uptake of drug molecules and ensuring their delivery to the appropriate cellular compartments.[47] In this study, we demonstrate that the uptake of TB511 by M2 macrophages is primarily mediated through CME and MP, but not through caveolae-mediated endocytosis. CD18, typically involved in receptor-mediated endocytosis such as CME, binds to a specific ligand, triggering the internalization of the receptor-ligand complex into the cell within a vesicle.[48] However, the role of CD18 in other forms of endocytosis, such as caveolae-mediated or clathrin-independent endocytosis, is not well established and may vary depending on the cellular context.[48 49] Therefore, it is plausible that in the case of our PDCs targeting M2 macrophages, CD18 is not involved in caveolae-mediated endocytosis. Although MP is a form of endocytosis that involves the non-selective uptake of extracellular substances, including fluids, solutes, and particles, various drug delivery systems can be internalized through this process.[50 51] Consequently, the cellular internalization strategy of TB511 targeting M2 macrophages through MP is expected to enhance the drug's efficacy. However, further research is needed to fully understand and optimize this process.

Following endocytosis, PDCs are typically enclosed in endosomes. Therefore, endosome escape refers to the process by which therapeutic agents, once internalized into a cell and sequestered within endosomes, are able to escape into the cytosol.[52] This is particularly crucial for drugs such as nucleic acid-based therapeutics, which must reach the cell's nucleus to exert their effects.[46] Without successful endosomal escape, these drugs can be degraded within the endosome or exocytosed from the cell, reducing their therapeutic potential.[53] In this study, we treated M2 macrophages with bafilomycin A1 (Baf-A1) and chloroquine (CQ), which are known to inhibit the acidification of early endosomes and prevent the maturation and fusion of endosomes and lysosomes for understanding the role of endosomal escape. Our results showed that treatment with Baf-A1 and CQ increased the colocalization of EEA1 and TB511-Cy5 in endosomes. In TB511, the dKLA peptide, known to facilitate endosomal escape as an antimicrobial peptide, can enhance endosomal escape through various strategies, including the use of pH-sensitive nanoparticles and liposomal complex systems.[54 55] Therefore, our findings suggest that TB511 is effectively internalized by M2 macrophages and can escape from the endosome into the cytosol. Importantly, we also observed that this treatment significantly decreased TB511-induced apoptosis, further supporting the importance of endosomal escape in the efficacy of TB511.

M2-TAMs within the TME play a significant role in cancer progression. These cells, which constitute a substantial portion of the stromal cells in the TME, exhibit an immunosuppressive phenotype and promote tumor growth, invasion, migration, and angiogenesis. Given their abundance and their roles in promoting cancer, M2 TAMs have emerged as potential targets for cancer

therapies.[15 56] Other studies have reported that targeting the CCL2-CCR2 axis increases the antitumor efficacy of $CD8^+$ T cells by interrupting the recruitment of macrophages to tumors.[57] Furthermore, targeting scavenger receptors with an anti-MARCO antibody increases NK cell activation and killing of tumor cells and has been shown to limit the immunosuppressive effects of M2-TAMs.[58] In this study, we showed that TB511 induces the inhibition of tumor growth by eliminating M2-TAMs in tumor tissues of NSCLC, CRC, RCC, TNBC, and pancreatic ductal adenocarinoma (PDAC). Targeting M2-TAMs by TB511 showed an increase of CD8 T and NK cells in tumor tissues and the activation of these cells by expressing GZMB and IFNG.

Recent studies have proposed therapeutic strategies that convert cold tumors into hot tumors to enhance the efficacy of immune checkpoint blockade (ICB) therapies.[59] These strategies aim to increase T cell infiltration into tumors, making them more responsive to ICB treatment. Our findings demonstrate that TB511 treatment leads to a significant increase in $CD8^+$ T cells and NK cells within the TME. This immune modulation suggests that TB511 may contribute to the transformation of cold tumors into hot tumors, potentially improving responsiveness to ICB therapies. Zhu *et al* reported that the combination of anti-CTLA4/anti-PD1 checkpoint inhibitors with CSF1/CSF1R blockade reduces $CD206^{hi}$ TAMs and reprograms macrophages to support antitumor immunity, resulting in improved checkpoint immunotherapy efficacy, ultimately leading to the regression of well-established PDAC tumors.[60] Since TB511 specifically targets M2-TAMs, its combination with ICB therapy may similarly enhance anti-tumor immune responses by reshaping the TME. Therefore, further studies are needed to evaluate the efficacy of TB511 in combination with ICB therapy.

CONCLUSIONS

In conclusion, our study identified CD18 as a target protein of TB511, which preferentially binds to M2 TAMs. We found that CD18 is highly expressed in its activated form due to conformational changes in M2 TAMs. Notably, CD18 demonstrated high expression and correlation with M2 macrophages in tumor tissues. Intriguingly, TB511 selectively targeted activated CD18 on M2 TAMs and induced cell death. This process was facilitated through the internalization of the drug via CME and MP, followed by subsequent intracellular endosome escape. Furthermore, in CRC and NSCLC mouse models, TB511 exhibited anticancer efficacy. This was accompanied by an increase in CD8 cells, achieved by eliminating M2 TAMs through CD18. Thus, our findings underscore the potential of activated CD18 on M2 TAMs as a promising new target for cancer therapy. Specifically, the ability of TB511 to target these cells highlights its potential as a promising therapeutic agent for cancer treatment. Furthermore, the anticancer efficacy of TB511 in a humanized mouse model demonstrated its potential for clinical applications in humans. Recently, TB511 has IND approval for a phase I trial (NCT06400160) in advanced solid tumors.

Author affiliations
[1]Department of Physiology, College of Korean Medicine, Kyung Hee University, Seoul, Korea (the Republic of)
[2]Department of Science in Korean Medicine, Kyung Hee University, Seoul, Korea (the Republic of)
[3]R&D Center, Twinpig Biolab Inc, Seoul, Korea (the Republic of)
[4]Department of Chemistry, Graduate School, Kyung Hee University, Yongin-si, Gyeonggi-do, Korea (the Republic of)
[5]GoPath Laboratories, Buffalo Grove, Illinois, USA
[6]Korean Medicine Application Center, Korea Institute of Oriental Medicine, Daegu, Korea (the Republic of)
[7]Department of Korean Medicine, College of Korean Medicine, Kyung Hee University, Dongdaemun-gu, Seoul, Korea (the Republic of)
[8]Department of Clinical Korean Medicine, Graduate School, Kyung Hee University, Seoul, Korea (the Republic of)
[9]Department of Biotechnology, Chonnam National University, Gwangju, Korea (the Republic of)
[10]Department of Applied Chemistry and Institute of Natural Sciences, Kyung Hee University, Yongin-si, Gyeonggi-do, Korea (the Republic of)

Acknowledgments We thank Seungbae Min for the graphic technical support, as well as Sihyun Park for technical support with methodology.

Contributors HB supervised the study. I-HH, SHK and HB conceived and designed. IC, HoC, SK, CJ, JY, YC, JC, HL, JSS, HDY, E-JL, NC, HG, SEL, SC, W-JL, MK, HK, SP, NP, EK, JHL and HoC performed the experiments and collected the data. I-HH and IC drafted the manuscript. I-HH, IC, HoC and D-SH performed the statistical analysis. All authors approved the final version of the manuscript. HB is the guarantor.

Funding This research was supported by the National Research Foundation of Korea (NRF) grant funded by the Korea government (MSIT) (RS-2023-00208347).

Competing interests HB, I-HH, H-SC, JC, HL and JSS are inventors of patents relating to TB511 (PCT/IB2022/051007, PCT/KR2023/004674, PCT/KR2023/004678) submitted by Twinpig Biolab. The other authors declare no competing interests.

Patient consent for publication Not applicable.

Ethics approval All animal experiments were performed with the approval of the Institutional Animal Care and Use Committee of Kyung Hee University (KHSASP(SE)-21-291 (LLC), KHSASP(SE)-22-453 (CRC), (KHSAP(SE)-20-308), and (KHUASP(SE)-S-22-493)).

Provenance and peer review Not commissioned; externally peer reviewed.

Data availability statement Data are available on reasonable request.

ORCID iDs
Ilseob Choi http://orcid.org/0000-0001-9698-0899
Hyunsu Bae http://orcid.org/0000-0002-0299-3582

REFERENCES

1 Simsek H, Klotzsch E. The solid tumor microenvironment-Breaking the barrier for T cells: How the solid tumor microenvironment influences T cells: How the solid tumor microenvironment influences T cells. *Bioessays* 2022;44:e2100285.
2 Li M, He L, Zhu J, *et al*. Targeting tumor-associated macrophages for cancer treatment. *Cell Biosci* 2022;12:85.
3 Tie Y, Tang F, Wei YQ, *et al*. Immunosuppressive cells in cancer: mechanisms and potential therapeutic targets. *J Hematol Oncol* 2022;15:61.
4 Peng L-S, Zhang J-Y, Teng Y-S, *et al*. Tumor-Associated Monocytes/Macrophages Impair NK-Cell Function via TGFβ1 in Human Gastric Cancer. *Cancer Immunol Res* 2017;5:248–56.
5 Xiao Y, Yu D. Tumor microenvironment as a therapeutic target in cancer. *Pharmacol Ther* 2021;221:107753.
6 Vinogradov S, Warren G, Wei X. Macrophages associated with tumors as potential targets and therapeutic intermediates. *Nanomedicine (Lond)* 2014;9:695–707.
7 Mantovani A, Marchesi F, Malesci A, *et al*. Tumour-associated macrophages as treatment targets in oncology. *Nat Rev Clin Oncol* 2017;14:399–416.
8 Fagerholm SC, Guenther C, Llort Asens M, *et al*. Beta2-Integrins and Interacting Proteins in Leukocyte Trafficking, Immune Suppression, and Immunodeficiency Disease. *Front Immunol* 2019;10:254.
9 Nourshargh S, Alon R. Leukocyte migration into inflamed tissues. *Immunity* 2014;41:694–707.
10 Sun H, Hu L, Fan Z. β2 integrin activation and signal transduction in leukocyte recruitment. *Am J Physiol Cell Physiol* 2021;321:C308–16.
11 Bednarczyk M, Stege H, Grabbe S, *et al*. β2 Integrins-Multi-Functional Leukocyte Receptors in Health and Disease. *Int J Mol Sci* 2020;21:1402.
12 Spada S, Tocci A, Di Modugno F, *et al*. Fibronectin as a multiregulatory molecule crucial in tumor matrisome: from structural and functional features to clinical practice in oncology. *J Exp Clin Cancer Res* 2021;40:102.
13 Cavalieri D, Dolara P, Mini E, *et al*. Analysis of gene expression profiles reveals novel correlations with the clinical course of colorectal cancer. *Oncol Res* 2007;16:535–48.
14 Li C, Deng T, Cao J, *et al*. Identifying ITGB2 as a Potential Prognostic Biomarker in Ovarian Cancer. *Diagnostics (Basel)* 2023;13:1169.
15 Xu H, Zhang A, Han X, *et al*. ITGB2 as a prognostic indicator and a predictive marker for immunotherapy in gliomas. *Cancer Immunol Immunother* 2022;71:645–60.
16 Balogh B, Ivánczi M, Nizami B, *et al*. ConjuPepDB: a database of peptide-drug conjugates. *Nucleic Acids Res* 2021;49:D1102–12.
17 Zhou J, Li Y, Huang W, *et al*. Source and exploration of the peptides used to construct peptide-drug conjugates. *Eur J Med Chem* 2021;224:113712.
18 Sui X, Niu X, Zhou X, *et al*. Peptide drugs: a new direction in cancer immunotherapy. *Cancer Biol Med* 2023;21:198–203.
19 Chavda VP, Solanki HK, Davidson M, *et al*. Peptide-Drug Conjugates: A New Hope for Cancer Management. *Molecules* 2022;27:7232.
20 Wang Y, Zhang L, Liu C, *et al*. Peptide-Mediated Nanocarriers for Targeted Drug Delivery: Developments and Strategies. *Pharmaceutics* 2024;16:240.
21 Brandsch M, Knütter I, Bosse-Doenecke E. Pharmaceutical and pharmacological importance of peptide transporters. *J Pharm Pharmacol* 2008;60:543–85.
22 Rubio-Aliaga I, Daniel H. Mammalian peptide transporters as targets for drug delivery. *Trends Pharmacol Sci* 2002;23:434–40.
23 Kim S, Choi I, Han IH, *et al*. Enhanced Therapeutic Effect of Optimized Melittin-dKLA, a Peptide Agent Targeting M2-like Tumor-Associated Macrophages in Triple-Negative Breast Cancer. *IJMS* 2022;23:15751.
24 Chakkarapani SK, Sun Y, Lee S, *et al*. Three-Dimensional Orientation of Anisotropic Plasmonic Aggregates at Intracellular Nuclear Indentation Sites by Integrated Light Sheet Super-Resolution Microscopy. *ACS Nano* 2018;12:4156–63.
25 Huang B, Wang W, Bates M, *et al*. Three-dimensional super-resolution imaging by stochastic optical reconstruction microscopy. *Science* 2008;319:810–3.
26 Chakkarapani SK, Sun Y, Kang SH. Ultrasensitive norovirus nanoimmunosensor based on concurrent axial super-localization of ellipsoidal point spread function by 3D light sheet microscopy. *Sensors and Actuators B: Chemical* 2019;284:81–90.
27 Marchuk K, Ha JW, Fang N. Three-dimensional high-resolution rotational tracking with superlocalization reveals conformations of surface-bound anisotropic nanoparticles. *Nano Lett* 2013;13:1245–50.
28 Kim Y, Cheong S-A, Lee JG, *et al*. Generation of knockout mice by Cpf1-mediated gene targeting. *Nat Biotechnol* 2016;34:808–10.
29 Blythe EN, Weaver LC, Brown A, *et al*. β2 Integrin CD11d/CD18: From Expression to an Emerging Role in Staged Leukocyte Migration. *Front Immunol* 2021;12:775447.
30 Pei D, Buyanova M. Overcoming Endosomal Entrapment in Drug Delivery. *Bioconjug Chem* 2019;30:273–83.
31 Xu D, He Y, Yeung ES. Direct imaging of transmembrane dynamics of single nanoparticles with darkfield microscopy: improved orientation tracking at cell sidewall. *Anal Chem* 2014;86:3397–404.
32 Chen K, Gu Y, Sun W, *et al*. Characteristic rotational behaviors of rod-shaped cargo revealed by automated five-dimensional single particle tracking. *Nat Commun* 2017;8:887.
33 Arnaout MA. Structure and function of the leukocyte adhesion molecules CD11/CD18. *Blood* 1990;75:1037–50.
34 Qu A, Leahy DJ. Crystal structure of the I-domain from the CD11a/CD18 (LFA-1, alpha L beta 2) integrin. *Proc Natl Acad Sci U S A* 1995;92:10277–81.
35 Wu X, Lahiri A, Sarin R, *et al*. T Cell–Extrinsic CD18 Attenuates Antigen-Dependent CD4+ T Cell Activation In Vivo. *J Immunol* 2015;194:4122–9.
36 Zhang K, Chen J. The regulation of integrin function by divalent cations. *Cell Adh Migr* 2012;6:20–9.
37 Cullere X, Lauterbach M, Tsuboi N, *et al*. Neutrophil-selective CD18 silencing using RNA interference in vivo. *Blood* 2008;111:3591–8.
38 Wen L, Moser M, Ley K. Molecular mechanisms of leukocyte β2 integrin activation. *Blood* 2022;139:3480–92.
39 Stelling MP, Soares MA, Cardoso SC, *et al*. Manganese systemic distribution is modulated in vivo during tumor progression and affects tumor cell migration and invasion in vitro. *Sci Rep* 2021;11:15833.
40 Usami Y, Ishida K, Sato S, *et al*. Intercellular adhesion molecule-1 (ICAM-1) expression correlates with oral cancer progression and induces macrophage/cancer cell adhesion. *Int J Cancer* 2013;133:568–78.
41 Zu L, He J, Zhou N, *et al*. The Profile and Clinical Significance of ITGB2 Expression in Non-Small-Cell Lung Cancer. *J Clin Med* 2022;11:6421.
42 Liu H, Wang J, Luo T, *et al*. Correlation between ITGB2 expression and clinical characterization of glioma and the prognostic significance of its methylation in low-grade glioma(LGG). *Front Endocrinol* 2022;13:1106120.
43 Mandal K, Wicaksono G, Yu C, *et al*. Structural surfaceomics reveals an AML-specific conformation of integrin β_2 as a CAR T cellular therapy target. *Nat Cancer* 2023;4:1592–609.
44 Ahn GO, Tseng D, Liao CH, *et al*. Inhibition of Mac-1 (CD11b/CD18) enhances tumor response to radiation by reducing myeloid cell recruitment. *Proc Natl Acad Sci U S A* 2010;107:8363–8.
45 Wang M, Liu J, Xia M, *et al*. Peptide-drug conjugates: A new paradigm for targeted cancer therapy. *Eur J Med Chem* 2024;265:116119.
46 Degors IMS, Wang C, Rehman ZU, *et al*. Carriers Break Barriers in Drug Delivery: Endocytosis and Endosomal Escape of Gene Delivery Vectors. *Acc Chem Res* 2019;52:1750–60.
47 Lindberg J, Nilvebrant J, Nygren P-Å, *et al*. Progress and Future Directions with Peptide-Drug Conjugates for Targeted Cancer Therapy. *Molecules* 2021;26:6042.
48 Khan I, Steeg PS. Endocytosis: a pivotal pathway for regulating metastasis. *Br J Cancer* 2021;124:66–75.
49 Rennick JJ, Johnston APR, Parton RG. Key principles and methods for studying the endocytosis of biological and nanoparticle therapeutics. *Nat Nanotechnol* 2021;16:266–76.
50 Jiang G, Wei C, Chen Y, *et al*. Targeted drug delivery system inspired by macropinocytosis. *J Control Release* 2023;359:302–14.
51 Liu H, Qian F. Exploiting macropinocytosis for drug delivery into KRAS mutant cancer. *Theranostics* 2022;12:1321–32.
52 Chen P, Yang W, Mochida Y, *et al*. Selective Intracellular Delivery of Antibodies in Cancer Cells with Nanocarriers Sensing Endo/Lysosomal Enzymatic Activity. *Angew Chem Int Ed* 2024;63.
53 Lee J, Sands I, Zhang W, *et al*. DNA-inspired nanomaterials for enhanced endosomal escape. *Proc Natl Acad Sci USA* 2021;118.
54 Lim C, Won WR, Moon J, *et al*. Co-delivery of d-(KLAKLAK)2 peptide and doxorubicin using a pH-sensitive nanocarrier for synergistic anticancer treatment. *J Mater Chem B* 2019.
55 Lim C, Kang JK, Won WR, *et al*. Co-delivery of D-$(KLAKLAK)_2$ Peptide and Chlorin e6 using a Liposomal Complex for Synergistic Cancer Therapy. *Pharmaceutics* 2019;11:293.
56 Zhu L, Li XJ, Gangadaran P, *et al*. Tumor-associated macrophages as a potential therapeutic target in thyroid cancers. *Cancer Immunol Immunother* 2023;72:3895–917.
57 Yang H, Zhang Q, Xu M, *et al*. CCL2-CCR2 axis recruits tumor associated macrophages to induce immune evasion through

PD-1 signaling in esophageal carcinogenesis. *Mol Cancer* 2020;19:41.
58 Eisinger S, Sarhan D, Boura VF, *et al*. Targeting a scavenger receptor on tumor-associated macrophages activates tumor cell killing by natural killer cells. *Proc Natl Acad Sci U S A* 2020;117:32005–16.
59 Duan Q, Zhang H, Zheng J, *et al*. Turning Cold into Hot: Firing up the Tumor Microenvironment. *Trends Cancer* 2020;6:605–18.
60 Zhu Y, Knolhoff BL, Meyer MA, *et al*. CSF1/CSF1R blockade reprograms tumor-infiltrating macrophages and improves response to T-cell checkpoint immunotherapy in pancreatic cancer models. *Cancer Res* 2014;74:5057–69.